5-1-2013

Development and validation of heat transfer model to predict indoor air temperatures in roofpond buildings

Afzal Hossain
University of Nevada, Las Vegas

DEVELOPMENT AND VALIDATION OF HEAT TRANSFER MODEL TO PREDICT INDOOR AIR TEMPERATURES IN ROOFPOND BUILDINGS

by

Afzal Hossain

Bachelor of Architecture
Bangladesh University of Engineering and Technology
2006

A thesis submitted in partial fulfillment
of the requirements for the

Master of Architecture

School of Architecture
College of Fine Arts
The Graduate College

University of Nevada, Las Vegas
May 2013

UNIVERSITY OF NEVADA LAS VEGAS

THE GRADUATE COLLEGE

We recommend the dissertation prepared under our supervision by

Afzal Hossain

entitled

Development and Validation of Heat Transfer Model to Predict Indoor Air Temperatures in Roofpond Buildings

be accepted in partial fulfillment of the requirements for the degree of

Master of Architecture
School of Architecture

Alfredo Fernandez-Gonzalez, M. Arch., Committee Chair

Daniel Ortega, M.L.A., Committee Member

Firas Al-Douri, Ph.D., Committee Member

Robert Boehm, Ph.D., Graduate College Representative

Tom Piechota, Ph.D., Interim Vice President for Research &
Dean of the Graduate College

May 2013

ABSTRACT

DEVELOPMENT AND VALIDATION OF HEAT TRANSFER MODEL TO PREDICT INDOOR AIR TEMPERATURES IN ROOFPOND BUILDINGS

by

AFZAL HOSSAIN

Alfredo Fernandez-Gonzalez, Examination Committee Chair
Associate Professor of Architecture
University of Nevada, Las Vegas

Roofponds mimic the ways in which nature tempers and controls the global climate; they utilize higher heat capacity of water to passively control the temperature of the interior space. From a thermal standpoint, roofponds are strong performers, providing high solar savings fractions, interior temperature stability, enhanced thermal comfort and very low operational power requirements. Moreover, due to convective heat transfer within the water bags, heat gains or losses are quickly distributed throughout the roofpond to create a very homogeneous distribution of heat throughout the floor area covered by the system.

Research by Harold Hay and John Yellott (Hay & Yellott, 1968) studied the feasibility of the roofpond system and tried to develop a heat transfer model for roofponds with insulation. During the late 1960s, several of their publications discussed the heating and cooling potential produced by various roofpond strategies. Throughout the 70's and 80's, a number of heat transfer models were developed to simulate different roofpond systems. Researchers at Trinity University tried to simplify the complexity of the simulation model without compromising the accuracy of its prediction. However, only a couple of them considered the whole building's heat transfer mechanisms.

This research intends to develop a model to predict the hourly indoor air temperatures in a single-zone building featuring a roofpond. Like most of the passive

design strategies, roofponds are difficult to model as they have; too many independent variables, mostly climatic parameters that influence the performance of the roofpond. However, the indoor air temperature of such a passive building (without mechanical conditioning systems) is highly influenced by the change in the daily outdoor air temperature profile as well as the incoming solar radiation. A transfer-function unsteady state model can predict the indoor air temperature of a roofpond building quite accurately. Such model can be greatly handy to design professionals for quick evaluation of such system during the early schematic design phase.

The study herewith presented uses data collected from a roofpond test cell located at the NEAT Laboratory of the University of Nevada, Las Vegas, and implements unsteady-state thermal heat transfer principles to predict average interior temperatures. The three distinct phases of the project are: **first**, to predict indoor air temperatures using transfer-function heat transfer equations; **second**, to statistically fine-tune the model by finding the correlation between the predicted and the measured temperature; and **third**, to validate the model using a different data set.

A thermal network model of the roofpond using the transfer-function method with a time step (ΔT) of one hour is used to calculate the indoor air temperature. Measured data of 14 days is used to develop the unsteady state heat-transfer model that can predict the average indoor air temperature. The predicted temperature then is regressed against the measured temperature to find the correlation. The cyclic patterns observed in residuals indicate the daily change in the outdoor temperature profile and imply that time-series model with Fourier series is apt for de-trending the pattern.

The model is then empirically modified to increase accuracy. Auto Correlation Factor (ACF) and Partial Auto Correlation Factor (PACF) tests suggested that either Auto Regressive (AR) or Auto Regressive Integrated Moving Average (ARIMA) model would

neutralize residuals. The empirically developed AR / ARIMA model is then added with the physical model to predict the interior air temperature. The AR (2) model which yielded the best fit model, was tested against data from another summer month for validation. The proposed validated hybrid model is capable of addressing the change in configuration of the roofpond building and can accurately predict the indoor air temperature.

ACKNOWLEDGEMENTS

All praise and thanks are due to ALLAH, The Most Gracious and The Most Merciful, for his great mercy bestowed on me.

This thesis is a result of many dedicated and wonderful individuals who provided their undivided support. I would like to acknowledge and express my gratitude and appreciation to Professor Alfredo Fernández-González, my advisor and chair, for his inspiration, support, and guidance. I could not have finished this research without his continuous encouragement and support. I would also like to thank my committee members, Professor Daniel Ortega, and Dr. Robert Boehm for their support and feedback. I would specially like to thank Dr. Firas Al-Douri for agreeing to join my committee on a very short notice.

I would also like to extend my gratitude to the team of researchers at the Natural Advanced Technologies (NEAT) Laboratory. I greatly appreciate my friends and my classmates for the support they provided throughout this journey and for understanding my devotion to this endeavor I chose. I am deeply indebted to my classmate Luke Doubravsky for his friendship and constant encouragement throughout my graduate study. A special thanks to Nazmul Islam, my lifelong friend, who has always believed in me and supported me.

I unconditionally thank my family – especially my mother, my sister and my grandparents. I owe my dearest mother my sincere gratitude for her love, guidance and prayers. I also like to thank my uncles and aunts for their love and support over the years. Last but not the least, I owe the deepest gratitude to my dearest wife, Shenjuti for her unconditional love, continuous encouragement and support ever since we got married. I would also like to thank her family as well for putting their trust in me. I ask ALLAH to reward them all and to shower them with His mercy and grace.

DEDICATION

To my mother and my grandparents,

for their love, guidance and prayers.

TABLE OF CONTENTS

LIST OF TABLES

LIST OF FIGURES

CHAPTER 1. INTRODUCTION

The use of water to achieve thermal comfort, especially to cool the built environment, is not a new concept. In fact, evaporative cooling has been used for the last several hundreds of years in Egypt and Iran (Cook, 1985). However, the use of water in the roof, in the form of a pond, is a relatively contemporary phenomenon and can be traced back to the 19th century (Givoni, 1994). The “Sebastopol House” in Seguin, Texas designed in 1850 by Colonel Joshua Young, is considered to be the first example of a roofpond building (Marlatt et al., 1984). This house utilized the higher heat capacity of water to passively control the temperature of the interior space. However, the concept of using a thermal storage roof in modern residential construction was pioneered by H. R. Hay in the early 60’s (Lord, 1999). Results from several of his experiments demonstrated the effectiveness of the roofpond in maintaining comfortable indoor temperatures throughout the year (Hay & Yellott, 1968). The roofpond system in the Atascadero House, built in 1973, was able to maintain interior temperatures between 62 ºF - 79 ºF (17 ºC – 26 ºC) without any backup heating or cooling, even though outside temperatures ranged from 26 ºF - 100 ºF (-3 ºC - 38 ºC) (Haggard, et al., 1975).

However, in spite of the documented energy savings produced by roofponds, as reported by Haggard et al. (1975), and the development of through design guidelines by Marlatt et al. (1984) roofpond system and other passive heating and cooling strategies failed to encourage the adaptation of such strategies in the United States where the vast majority of the buildings use mechanical systems for heating or cooling interior spaces (Fernandez-Gonzalez, 2007). Nevertheless, an increased awareness of the negative effects produced by the increasing consumption of non-renewable energy in buildings has brought about renewed interest in roofpond buildings. This has resulted in several

experimental studies undertaken recently to validate and further characterize the heating and cooling performance of roofponds (Hossain & Fernandez-Gonzalez, 2012).

1.1 Research objective

The objective of the research conducted within the scope of this Master of Architecture thesis is to study how heat is gained and/or lost by the water mass of a roofpond building. The research intends to investigate how climatic parameters such as solar insolation and outdoor air temperature influence the heat transfer through the water mass. This investigation is the basis for understanding the causal-relationship between these climatic parameters and the indoor air temperature in buildings using roofpond systems. Like most of the passive design strategies, roofponds are difficult to model physically as they have too many independent variables, mostly climatic parameters, which influence the thermal performance of the building. The intent of this research is to develop, fine-tune, and validate a thermal network model for a dry roofpond system that can be used to predict the interior average temperature of a roofpond building.

1.2 Significance of the research

With 6% of the world population, the United States accounts for 32% of the world's energy consumption. In 2009 the residential and commercial building stock consumed 41% of the total energy used in the U.S (Figure 1 & Figure 2). However, the entire U.S. building stock, which includes residential, commercial and industrial buildings and their construction materials including their production and processing, accounts for 46% of all the energy consumed by the country each year costing $350 billion per year (EIA, 2010). Hunn (1996) recognizes that between 1950 and 1987 the U.S. population increased by

50% while the energy consumption by its building stock doubled. Between 1949 and 2009 primary energy consumption by the U.S. building stock nearly tripled (EIA, 2010). Furthermore, residential building stock is responsible for 22% of all U.S. CO_2 emissions annually and it is also the fastest growing energy-consuming and CO_2 emitting sector within the U.S. (Mazria, 2003).

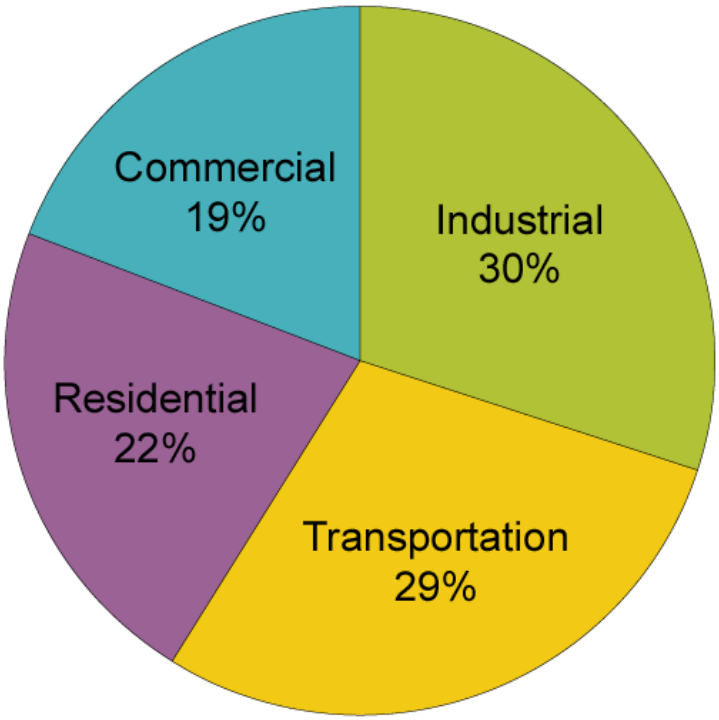

Figure 1: Share of energy consumption by major sectors of the economy (Source: EIA, 2010)

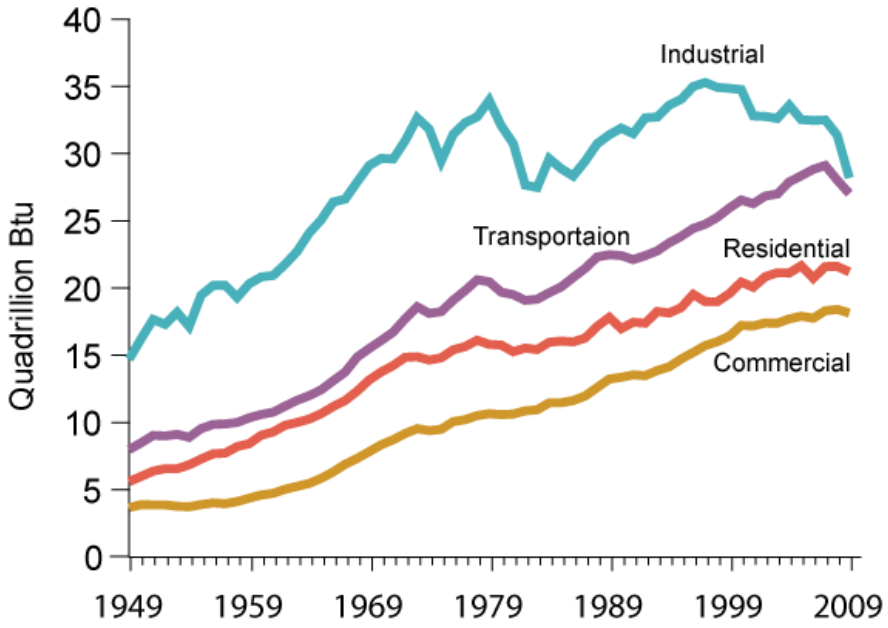

Figure 2: Energy consumption by sector (Source: EIA, 2010)

While there are numerous factors influencing the increased dependency on energy, it can be partially attributed to the fact that modern residential buildings have been, almost entirely, depending upon the availability of mechanical heating and cooling systems. As a matter of fact, mechanical air-conditioning is considered one of the most important accomplishments of modern building technology. Such a mindset led the profession of architecture to a *status quo* design practice that disregarded the climate as a design determinant, resulting in no or very little concern for conserving energy or, for that matter, sustainability of the built environment. Consequently, more and more buildings have been added to the U.S. building stock with poor thermal performance properties.

On the other hand, passive design strategies have been practiced throughout the span of human civilization across the world and have produced buildings that consumed less energy, require low maintenance, and yet achieve superior comfort level (Mazria,

2003). Passive strategies employ building design techniques that avoid outdoor heat gain and transfer indoor heat to natural heat sinks (Cook, 1985). Roofpond systems, defined as a passive solar strategy in which both heating and cooling occur through the use of natural environmental forces, are no exception to that and show similar traits (Marlatt et al., 1984).

In 1982, Marlatt et al. reported a month-long study of roofpond systems. Their study found that in cities with high sensible cooling loads and small latent loads like those found in the dry regions of the US southwest (*e.g*. Phoenix), energy savings of 50-70% can be expected with dry-roofponds and savings of 87-97% can be achieved with wetted surface roofpond buildings, when compared with traditionally air-conditioned houses. In cities with low sensible cooling loads and nonexistent latent loads (*e.g.* Albuquerque), a roofpond performs substantially better and a dry-roofpond alone would provide the 100% of the cooling requirement. However, in cities where cooling loads are mostly latent (*e.g*. Atlanta), the performance of roofpond systems drops significantly. In such climate, a dry roofpond would reduce energy consumption by only 25-50%, and the wet roofpond would add only minimal cooling effect. In climates with an outdoor air temperature that ranges between 32 - 80 °F (0 - 27 °C), well-designed roofpond buildings can maintain 60 - 80 °F (16 - 27 °C) without HVAC system (Marlatt et al., 1984).

However, Marlatt et al. also reported that in spite of well documented energy savings produced by roofponds, by 1985 there were less than 20 buildings designed employing roofponds, the majority of which were test facilities. The slow implementation of roofpond systems can be attributed to limited public and architectural acceptance of the technology, seemingly high initial costs compared to conventional buildings, lack of standardized or modular components, the need for high degree of quality in

workmanship, and increased maintenance costs for the residential applications. Moreover, in case of existing buildings design considerations involved in placing a large mass of water above the living space preclude any significant potential for retrofits (Hoffstatter, 1985).

Some of the advantages of roofpond buildings over conventional residences reported by Marlatt et al. (1984) are:

- A roofpond system can provide both heating and cooling with no alternation of system components.
- In both heating and cooling modes roofpond system outperforms any other passive systems, when employed alone.
- A roofpond building will save a substantial amount of energy for heating and cooling compared to traditionally conditioned buildings.
- Roofpond buildings provide more even temperature compared to the traditional buildings.
- Since air motion is not required for heating and cooling of a roofpond building, the noise from blowers and air conditioners is eliminated.
- Since heat is transferred by radiation in a roofpond building, no excessive air movement is present due to fans or blowers.

CHAPTER 2. LITERATURE REVIEW

2.1 Roofpond: Definition and characteristics

2.1.1 Roofpond strategy for passive cooling and heating

A roofpond uses water as thermal mass that is located on the roof of a building (Mazria, 1979). This strategy utilizes the higher heat capacity of water to mediate the temperature of the interior space beneath. It mimics the ways in which Mother Nature tempers and controls the global climate. Therefore, roofponds can be defined as a passive solar strategy in which both heating and cooling occur through the use of natural environmental forces (Marlatt et al., 1984). This passive solar strategy is the only one that has the ability to both heat and cool without additional system components (Hay & Yellott, 1968). From a thermal standpoint, roofponds are strong performers, providing high solar savings fractions, interior temperature stability, enhanced thermal comfort and very low operational power requirements (Hoffstatter, 1985). Moreover, due to convective heat transfer within the water bags, heat gains or losses are quickly distributed throughout the roofpond to create a very homogeneous distribution of heat throughout the floor area covered by the system (Haggard et al., 1975).

2.1.2 Roofpond types

The traditional roofpond consists of horizontally-oriented thermal storage (water) placed at the roof level of a building with a flat-roof (Figure 3). The surface of the roof is constructed of highly conductive metallic surface to enhance heat transfer (Mazria, 1979). Based on how water is contained on the roof, roofponds can be classified in three types: *dry roofpond, wet roofpond,* and *open roofpond*.

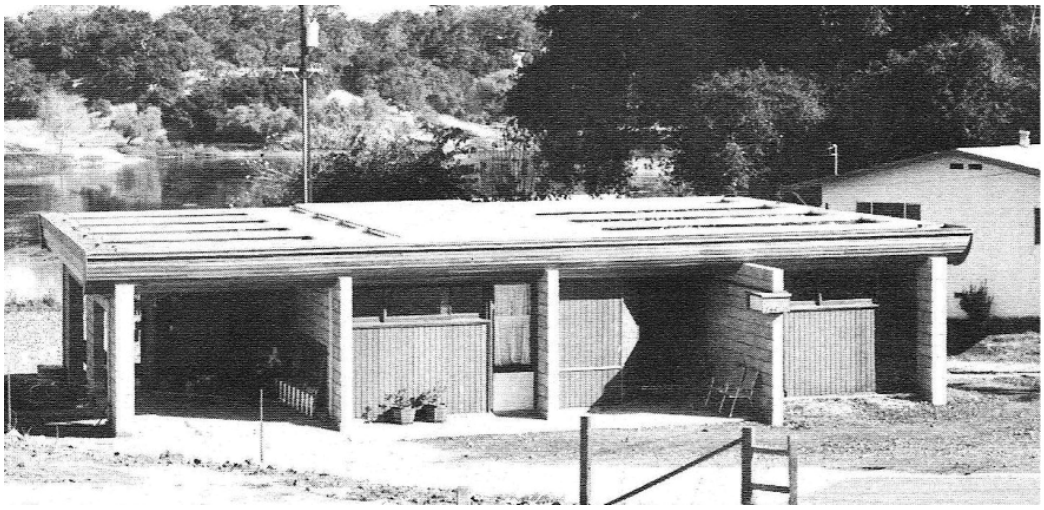

Figure 3: Atascadero House - the first residential prototype to incorporate a roofpond system (Mazria, 1979)

In a **dry roofpond** water is kept enclosed within transparent polyethylene bags and does not circulate in and out of the bags at any time. The water bags are spread over the entire roof and supported by the structural ceiling. Highly conductive metal decking is generally used as the structural ceiling. Dry roofpond systems might also consist of movable insulation panels that cover the water bags at appropriate times during both the heating and cooling modes of operation. Dry roofponds may or may not be glazed and can be adapted for both cooling and heating applications (Marlatt et al., 1984).

In a **wet roofpond**, water is contained in transparent bags that are flooded or sprayed with water so that surfaces of bag remain wet. Since this strategy greatly enhances the cooling performance of the roofpond by incorporating evaporative cooling they are most suitable for cooling purposes. However, the system might be adaptable for heating as well, by draining out the flooded/sprayed water (Marlatt et al., 1984).

Open roofpond systems are used only for cooling applications where water is kept exposed as an open pool. Lack of thermal protection during the heating mode makes such configurations prone to extensive heat loss to the night sky (Marlatt et al., 1984).

Roofponds can also be categorized into two types based on the configuration of their structure: *exposed roofpond*, and *enclosed roofpond*. In **exposed roofpond** systems, moveable insulation panels are placed on top of the water mass that act as a barrier between the pond and the environment. This configuration can be effectively used in both heating and cooling application and can be employed with dry, wet as well as open roofponds. On the other hand, in **enclosed roofpond** systems water mass is completely enclosed in attic space of clerestory type roof. The clerestory acts as a permanent barrier between the pond and the environment. Such configuration is advantageous for applications where heating loads predominate and dry roof ponds are employed (Marlatt et al., 1984).

2.1.3 Thermal principles of roofpond systems

In **heating mode** (Figure 4), the movable insulation panels are retracted and the sealed water bags are exposed to solar radiation during the daytime. The water stores much of the thermal energy absorbed from the incident solar radiation, evenly distributing it throughout the roofpond by means of convective heat transfer. Absorbed heat is then radiated to the occupied space below. In the evening, or in case of inadequate solar radiation during the daytime, the movable insulation covers the water mass to minimize the radiation heat loss to the sky. The radiant heat transfer from the roofpond to the occupied space below remains effective until temperature equilibrium is reached between the roofpond and the interior occupied space.

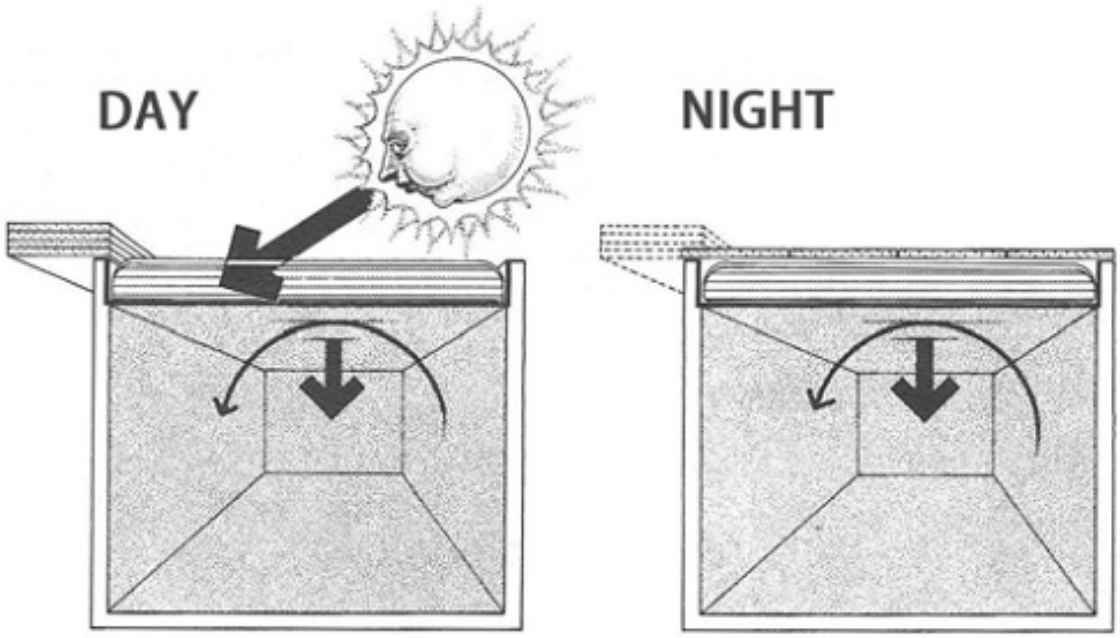

Figure 4: Roofpond heating mode (Mazria, 1979)

In **cooling mode** (Figure 5), the movable insulation panels are positioned over the water bags in order to reduce heat gain from incident solar radiation and the hot outdoor air. Since the occupied space below persistently gains heat throughout the day, the roofpond acts as a heat sink and tends to withdraw heat from the occupied interior space. At night, when the environment is able to absorb unwanted heat from the roofpond, the movable insulation panels are retracted. At this time, the roofpond radiates to the sky the heat absorbed and accumulated during the daytime.

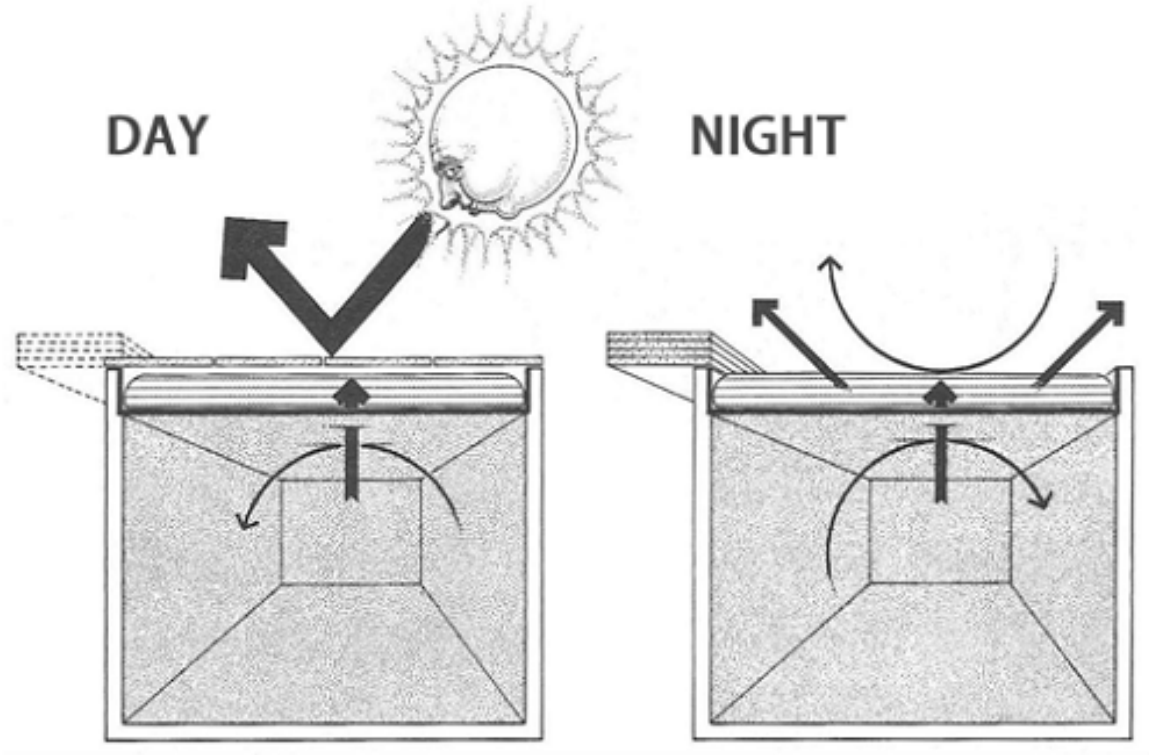

Figure 5: Roofpond cooling mode (Mazria, 1979)

2.1.4 Climatic attributes of roofpond systems

The performance of roofpond systems is affected primarily by climatological factors: insolation, outdoor ambient temperature, absolute humidity, cloud cover, and wind velocity. **Insolation** is the total amount of solar radiation (direct, diffuse, and reflected) striking an exposed surface (Mazria, 1979). It is expressed as the rate at which solar radiation directly falls on a horizontal surface. At higher latitudes, where heating loads are more demanding, solar radiation strikes the water mass at low angles, reducing heat absorption. Though the large collection area of the roofponds can overcome the low irradiation rate, the horizontal position of the pond essentially hinders solar collection to

a great extent. However, performance can be increased by using reflectors to direct incoming radiation onto the surface of the pond (Marlatt et al., 1984).

Outdoor ambient air temperature determines the number of heating and cooling degree days which influences the design of roofpond houses. As a rule of thumb, the greater the number of heating degree days, the more heating must be supplied by the roofpond. Alternately, the greater the number of cooling degree days, the more heat must be removed from the roofpond. Hot-arid climates like the one found in the U. S. Southwest are ideally suited for exposed roofpond systems which provide more cooling, whereas the Northern U.S., having short cooling seasons, requires enclosed roofpond systems that emphasize heating. Warm air temperatures limit the cooling capability of the roofpond and actually might add heat to the water mass if the temperature of the pond is below the ambient temperature. In heating applications, colder air temperature increases the heat lost by the roofponds (Marlatt et al., 1984).

Absolute humidity of the outside air greatly influences the magnitude of evaporative and radiative cooling. Mazria (1979) reports that up to 20-30 Btu/h.ft^2 of heat can be dissipated every hour under the clear sky condition with lower humidity level and cool nighttime temperatures. On the other hand, a high humidity level lowers the rate of radiative cooling by increasing the effective temperature of the night sky and by inhibiting evaporative cooling by limiting the amount of additional moisture that may be added to the atmosphere. Effectiveness of evaporative cooling greatly decreases with the increase of absolute humidity; however it is still effective in offsetting the decreased capacity for radiative cooling (Marlatt et al., 1984).

Cloud cover during the daytime reduces the amount of direct radiation incident on the ponds and thus reduces the heating performance of the system. Consistently cloudy or foggy weather will provide insufficient solar radiation resulting in inefficient roofpond

application. Likewise, cloud cover also affects the effectiveness of the roofponds during the nocturnal cooling mode as the presence of cloud increases the night sky temperature and inhibits radiative cooling of water mass. Since radiative cooling is the primary mechanism for cooling roofpond, the greater the area of cloud coverage, the less effective will be the cooling performance of the roofpond (Marlatt et al., 1984).

Wind velocity as well as wind direction influences the convective heat transfer co-efficient and thus affects the magnitude of heat-exchange between the roofpond surface and the environment. During the summer, wind assists cooling by means of convection, provided that the air temperature is below the pond temperature. In winter, however, prevailing winds impede the heating performance of the roofpond by increasing the convective heat transfer. In general, wind currents across the roofpond surface should be maximized in regions with high cooling loads and minimized in regions where high heating loads predominate (Marlatt et al., 1984).

2.2 Chronological development of roofpond research

Although passive solar heating and cooling strategies have been used extensively throughout history with great success, systematic research on passive cooling is a relatively recent phenomenon (Givoni, 1994). Heat flux reduction through the roof was probably first investigated at the University of Texas in the 1920s (Cook, 1985). By the 1930s, roofs with a water pond on top were used but only to provide cooling to the interior spaces of a building. However, insulation panels were not used at that time to further enhance the cooling potential of roofponds. Heating potential of such arrangement was not thoroughly explored (Marlatt, Murray, & Squier, 1984). During 1940s, several researchers were investigating the cooling efficiency provided by open pond systems (Spanaki, 2007). However, the roofpond concept gained acceptance as a

practical and feasible approach due to the work of Harold Hay (Marlatt, Murray, & Squier, 1984). Hay began his experiments with roofpond systems in 1954, in New Delhi, India and recognized the potential of using movable insulation to shield or expose the water mass that overcome both overheating and excessive cooling. Along with John Yellott, Hay was able to experimentally determine the practicality of external movable insulation for both open and closed roof ponds. During the late 1960s, a number of publications by Harold Hay and John Yellott discussed the heating and cooling potential produced by various roofpond strategies (Hay & Yellott, 1968).

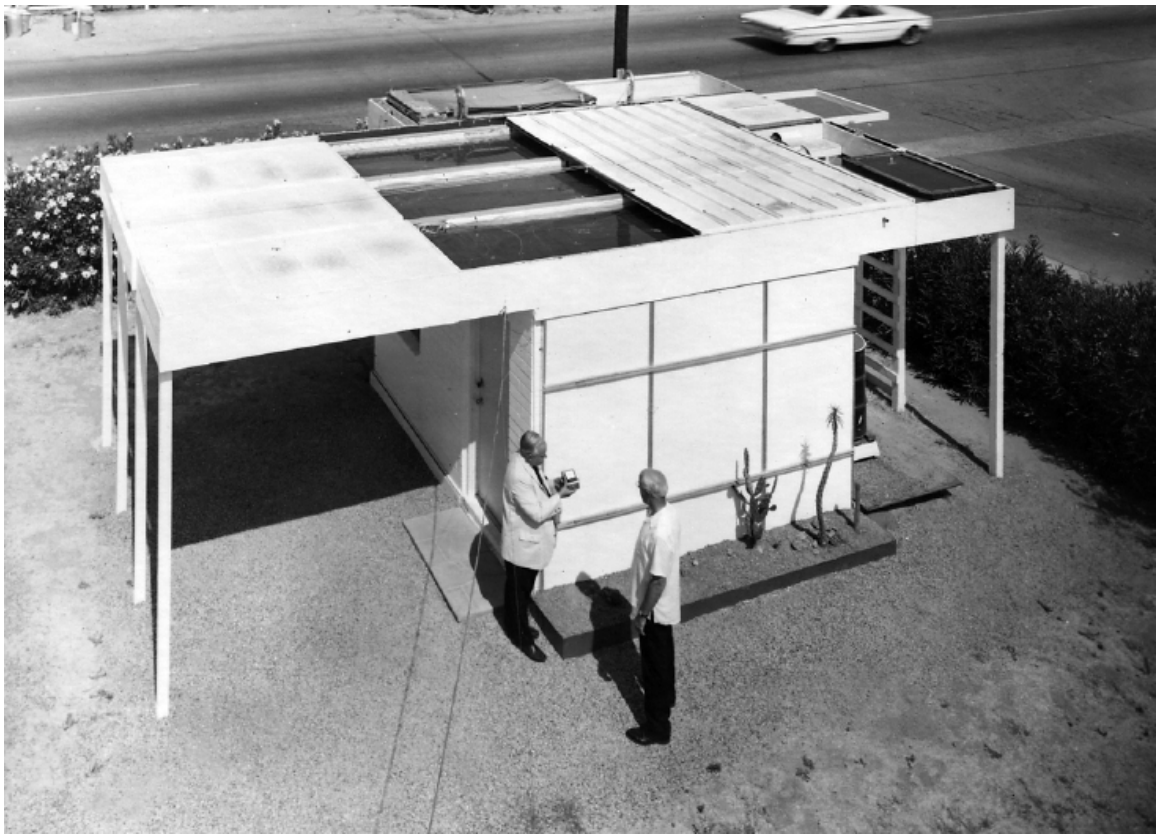

Figure 6: First Skytherm™ prototype built in Phoenix, AZ (Hay & Yellott, 1968)

In 1967 Hay constructed the Skytherm™ prototype that employs movable insulation panels to increase the efficiency of the roofpond system (Figure 6). The system was invented and patented by Hay. The first Skytherm™ prototype was built in Phoenix, Arizona to demonstrate the effectiveness of the thermal storage roof in maintaining comfortable indoor temperatures throughout the year (Lord, 1999). The yearlong experiment manifested that the strategy can perform well in the United States Southwest without supplementary heating and cooling. The prototype maintained an indoor air temperature inside the building between 68 ºF and 82 ºF (20 ºC and 27.8 ºC).

Figure 7 illustrates the relationship between the indoor air temperatures maintained by the prototype and their corresponding outdoor ambient air temperature that spanned from subfreezing to over 110 ºF (43.3 ºC).

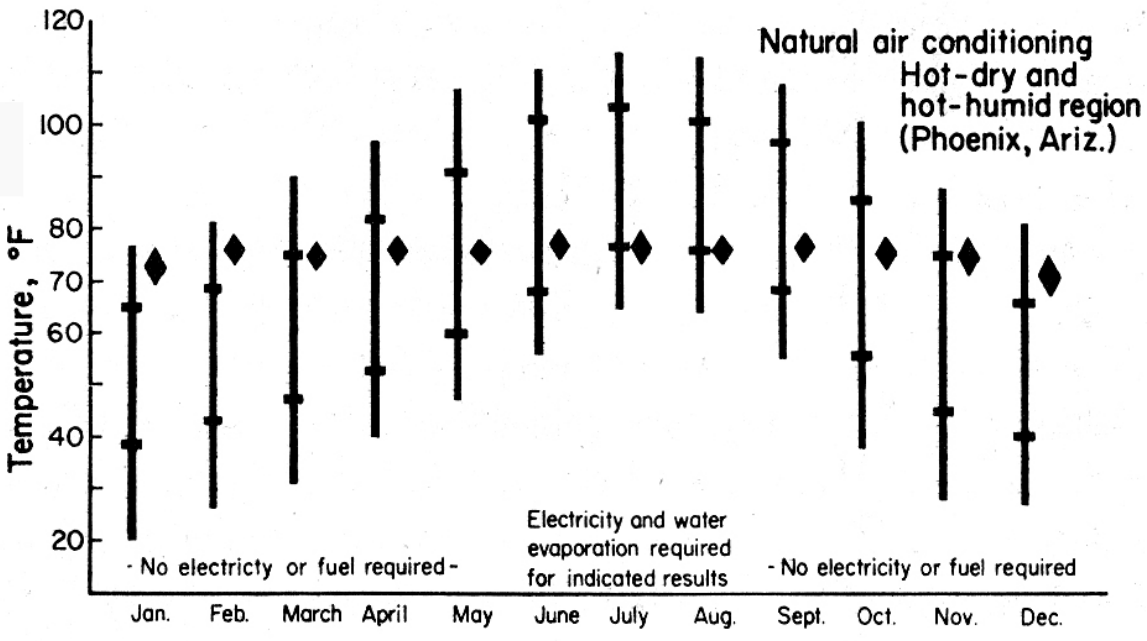

Figure 7: Phoenix prototype thermal performance data (Hay & Yellott, 1968)

Following the encouraging outcomes from this Phoenix prototype, in 1973 Harold Hay and Kenneth Haggard built a 1,192 ft^2 single family residence in Atascadero, California (Figure 3) to evaluate the thermal performance of the roofpond system (Marlatt et al., 1984). Haggard et al. (1975) reported that the thermal performance of the Atascadero House was extremely positive as the roofpond with the moveable insulation panel was able to supply all the heating and cooling requirements during the test months. During this period, the system was able to keep the indoor temperature between 66 ºF and 74 ºF. The interior temperature profile for a heating day (Figure 8) and a cooling day (Figure 9) was found to be very steady (Mazria, 1979). Though the study did not report the thermal perfomance for the months of November, December and January, extrapolaiton from a cmputer simulation model showed that the system would have kept he indoor temperature above the 66 ° F (Haggard et al., 1975).

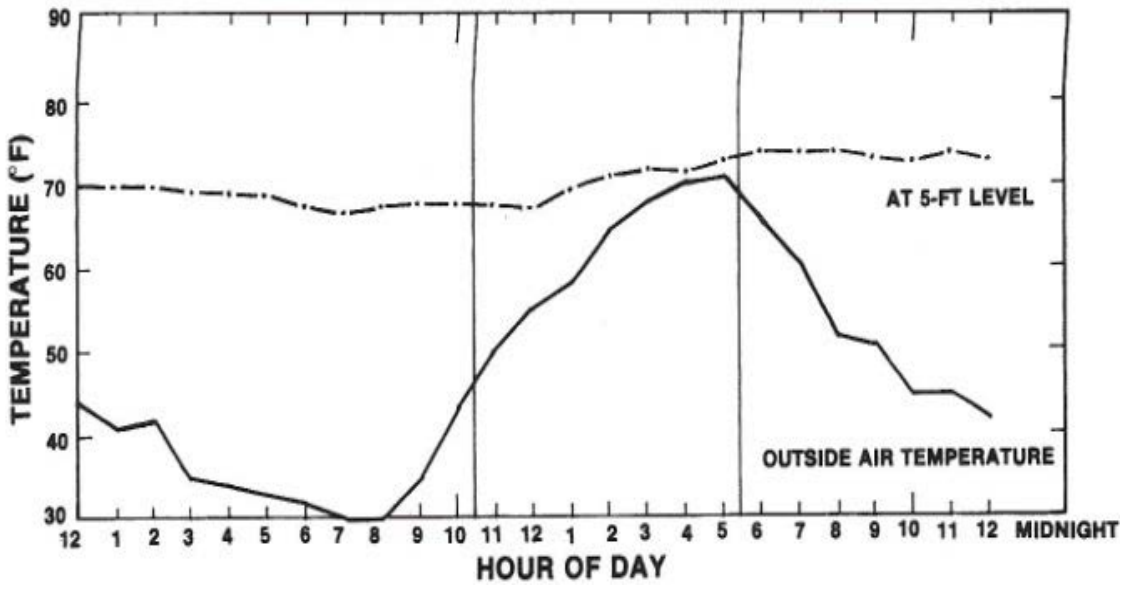

Figure 8: Typical heating-day performance of Atascadero house roofpond system (Source: Mazria, 1979)

However, the infinite-mass analytical model, developed by Haggard et al. was over simplified and considered that the capacitances of the walls, slab and windows were infinitely larger (Haggard et al., 1975). Later, Niles and colleagues developed a steady periodic sinusoidal model for predicting steady-state temperatures and the magnitude of the temperature swing; the model was applied to the Atascadero house with good results (Haggard et al., 1975). Several other Skytherm™ prototypes were constructed during the 1970s to evaluate both heating and cooling performance of roofpond buildings throughout the United States (Haggard et al., 1975).

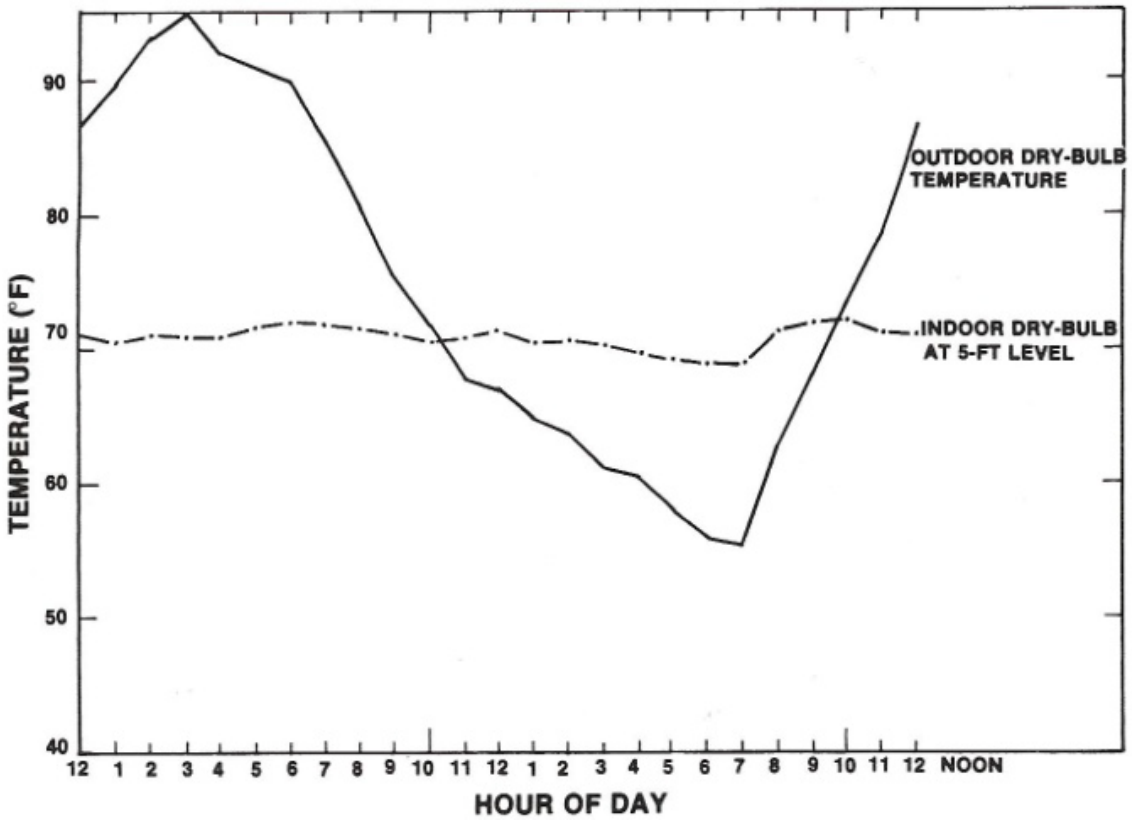

Figure 9: Typical cooling-day performance of Atascadero house roofpond system (Source: Mazria, 1979)

By the end of the 1970s several researchers started to explore mechanisms that can enhance the cooling effect. One of the very first strategies was to use a shaded pond of water over the roof and circulating the pond water through the room (Crowther & Melzer, 1979; Norton & Probert, 1983). Around the same time Sodha and colleagues proposed a novel concept of flowing water over the roof to reduce the heat flux (Sodha et al., 1980). In the following years, Sodha and other colleagues proposed to replace the spray system with wet gunny-bags to minimize the construction cost as well as to reduce maintenance requirement (Sodha et al., 1981). However, most of the research did not account for the heat transfer through the building envelope until Chandra and colleagues proposed the consideration of the whole building heat transfer mechanism for roofpond buildings (Chandra et al., 1985). An experiment by Ahmed in 1985 studied the evaporative cooling performance of the roofpond systems and reported improved cooling efficiency of the system (Ahmed, 1985). Later on, Carrasco tried to incorporate the effect of emissivity and used a system with low emissive construction materials. The use of low-emissive materials along with the roof spray system resulted in significant reduction of ceiling temperature (Carrasco et al, 1987).

Although the concept of using roofponds received increased momentum by the end of the decade, the advantages of evaporative cooling were mostly neglected (Verma et al., 1986). Most of the evaporative cooling techniques were put into practical use during the 90's. Among different roof evaporative cooling techniques, roofs covered with wet gunny-bags and ponds with a movable insulation were widely considered as the most efficient systems for cooling of buildings (Tiwari et al., 1993). Nevertheless, the unreliable mechanical system of the latter strategy proved to be decisive as researchers were skeptical about its success (Nahar et al., 1999).

More recently researchers at Ball State University resumed research on dry roofpond configuration (Fernandez-Gonzalez, 2007). Researchers at the University of Nevada, Las Vegas started research on Skytherm™ system and introduced automated movable panels (Fernandez-Gonzalez & Hossain, 2010).

2.3 Review of previous roofpond research

The infinite-mass heat transfer model developed by Haggard et al. (1975) was over simplified considering the capacitances of exterior surface to be infinitely large thus overpredicting the performance. The model developed by Niles et al. (1975) was able to predict only the steady-state temperature. Models developed by Crowther & Melzer (1979) and Norton & Probert (1983) were designed to predict the temperature for a configuration that is different from the traditional Skytherm™. Sodha et al. (1980, 1981) developed a model to predict indoor temperatures utilizing a roofpond system with evaporative cooling.

At Trinity University, Clark et al. (1983) developed an assessment tool for roofpond systems. The computer simulation tool was developed based on theoretical equations. In developing the computer simulation tool, Clark et al. (1983) first identified the three possible modes of heat transfer between the top surface of the roofpond and the outside environment: radiation, convection, and evaporation. Schutt (1984) identified the relevant heat transfer equations and used the same heat transfer model proposed by Clark et al. and tried to predict the heat loss from the top surface of the pond. He hypothesized that if the difference between measured and simulated heat losses exceeded the experimental error then the simulation would have to adjust to minimize the difference. For simplicity his simulation treated the pond as being uniform in temperature and heat flux. One significant observation from his study was that the

simulation over-predicted the rates of heat loss at lower heat loss rates and under-predicted them at higher heat loss rates. The error associated with the use of meteorological wind speed was also significant in directing the future research. However, the study focused only on nocturnal cooling and did not address daytime cooling (or heating). The model overlooked the effect of infiltration which also contributes significantly in thermal balance of any real building.

Though the assessment indicated that roofponds could provide a significant portion of residential cooling loads for warm-humid climates, the computer simulation was full of uncertainties (Schutt, 1984). Schutt recognized that the theoretical equations used in the simulation were developed for heat transfer from a solid surface but how well they could be used to model the heat transfer from flexible and fluid surfaces was not examined. Several other researchers at Trinity University also tried to validate the simulation program to use the model to accurately predict the performance of roofponds in any location for which accurate meteorological data are available (Hoffstatter, 1985).

Hoffstatter (1985) pushed the boundary of the scope of the previous two research studies and focused on heat transfer for the heating mode. His study also incorporates the effect of inflated glazing layer that increases the heating effectiveness of the roofpond system. Similar to the other two Trinity University research studies, however, Hosffstatter's study uses steady-state, one-dimensional heat transfer, and transient heat transfer was left unaddressed. Moreover, similar to its predecessor, the experiment did not take into account heat transfer through the building envelope, limiting its effectiveness in a practical situation. Models developed at the Trinity University by Clark et al. (1983), Schutt (1984), and Hoffstatter (1985) were based on the theoretical equations and more applicable for the Skytherm™ roofponds. However, the biggest concern was the higher level of uncertainties of the computer simulation model.

A thermal heat balance model that considers the whole building heat transfer mechanism for roofpond buildings was first proposed by Chandra et al. (1985). Chandra et al. (1985) modified the model developed at the Trinity University and took into consideration the whole building heat transfer mechanism; the model was also applicable only for roofponds with evaporative cooling. However, their study focuses on different evaporative cooling configurations and did not address radiative cooling. However, none of these studies distinguishes between radiative, convective and evaporative cooling. Chen et al. (1988) sought to separate the radiative cooling from the convective-evaporative components of heat transfer to simplify the heat balance model. Very recently, Jain (2006) developed a thermal model for roofponds in the arid region of Rajasthan, India.

In the early 1980's, despite the fact that roofponds, and passive heating and cooling strategies in large, can save energy federal research funding in the United States was cut and research on passive solar strategies stopped. Interest in passive strategies faded away and no significant experimental research on roofpond was conducted for almost two decades. During this period no significant research was conducted on roofpond system. Researchers such as Balcomb (1992) wrote extensively on passive design strategies and compiled the research on roofpond systems. During this time Givoni (1994) was developing empirical models for passive design strategies including roofpond system using minimal climatic information. These models have higher accuracy in predicting indoor air temperature but they are incapable of addressing configurationally changes in the system (Givoni, 1999).

In the early 2000's, however, experimental research on roofpond resumed in Ball State University (Fernandez-Gonzalez, 2007). Around the same time researchers at California Polytechnic State University were also conducting experimental research on

roofpond and developed physical model for the dry roofpond systems (Lord, 1999). In 2004 researchers at the University of Nevada, Las Vegas started research on dry roofpond configuration having automated movable insulation panel (Fernandez-Gonzalez & Hossain, 2010). Researchers at the Natural Energies Advanced Technologies Laboratory in University of Nevada, Las Vegas also focused on deriving empirical models to predict the indoor maximum, average, and minimum temperatures in roofpond buildings using minimum climatic information (Kako, 2009).

The proposed research intends to develop a thermal heat transfer model applicable for the dry roofpond systems. The model will take into consideration the effect of whole building heat transfer mechanism of a roofpond building, as proposed by Chandra et al. (1985). The first step is to identify the thermal network that represents the heat transfer mechanism of a dry roofpond system. The thermal network will be used to develop a physical model to predict indoor air temperature. In the next step the model will be statistically fine-tuned to increase the accuracy of the model. Both the physical model and the empirical model will then be combined to develop a hybrid model that has the flexibility of a physical model and the accuracy of an empirical model.

CHAPTER 3. METHODOLOGY

3.1 Research design

The proposed research will employ an experimental research design to determine the causal relationship between the independent variable and dependent variables. The experiment will use data from a roofpond test cell that contains water-mass on top of its ceiling. Data collected from the test cell are used to determine the heat transfer through the pond itself. Heat transfer through the ceiling and the water mass of the roofpond test cell fluctuates with the changing ambient air temperature, solar radiation, wind speed, and absolute humidity, but most importantly, by the characteristics of the water-mass. However, since the outdoor dry-bulb temperature and solar insolation impact the dependent variable the most, the effects of wind speed and absolute humidity were not included in the research design to negate the impact of cofounding variables.

Table 1. List of variables

Variable type	Name of the variable	Unit	Description
Dependent variable	Interior air temperature	°F (°C)	Fluctuates with the magnitude of heat transfer through the water-mass
	Interior Ceiling temperature	°F (°C)	
Independent variable	Exterior air dry-bulb temperature (DBT)	°F (°C)	Climatological parameter, changes over time both diurnally & seasonally
	Solar insolation	Btu / h.ft^2 (W / m^2)	

The calculated heat transfer value for the water-mass can then be used to statistically determine (regression analysis) its correlation with the climatic parameters (independent variable). This helps to find the individual effect of each of the independent variables.

Once the most significant variables are distinguished, the next step would be to establish a mathematical model using the general heat transfer equations (Figure 10).

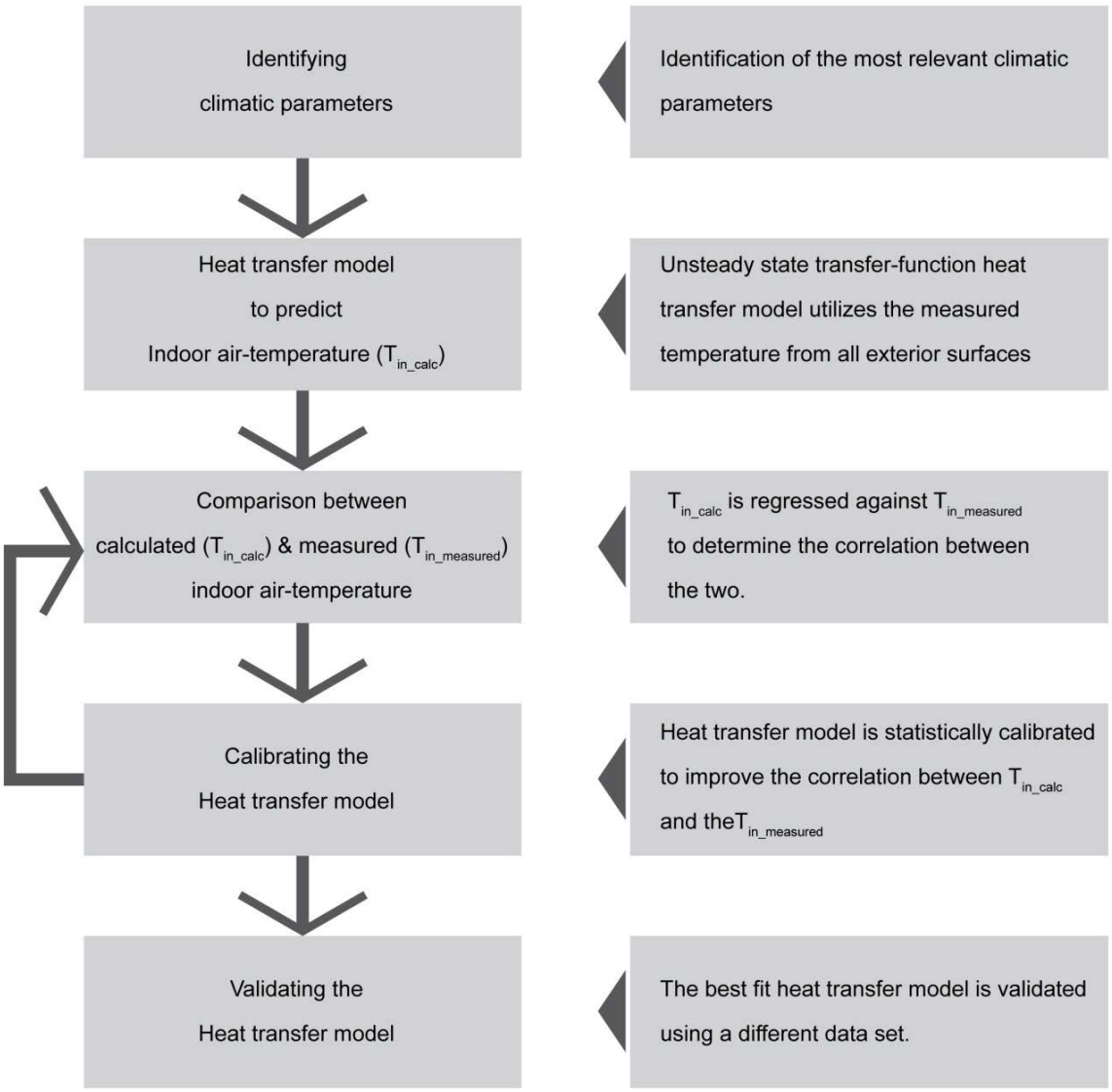

Figure 10: Conceptual diagram for the research framework

Determination of heat transfer through the water-mass is essential in predicting the interior air temperature changes. The magnitude of the heat transfer varies with the

change in climatological parameters, which in turn varies with the diurnal as well as seasonal change. Therefore, the proposed research study intends to employ time sampling.

To represent the seasonal changes in climatological parameters, data for one summer month (cooling mode) and one winter month (heating mode) were collected. Determination of the two representative months was based on solar insolation, outdoor ambient temperature, wind speed, etc. that are considered representative of a typical winter and a summer month. This weather data was collected from a weather station installed very next to the experimental setup. However, typical Meteorological Year (TMY) data, available from the U.S. National Renewable Energy Laboratory (NREL) website is also used occasionally to compare with the weather data collected at the site.

Data for an extended period of time (one month) were measured, collected, and compared to capture a greater variation in climatological parameters so to increase the *validity* of the experimental setup. The embedded limitations corresponding to the scope and attributes of the experimental setup greatly affect the generalizability of the findings. The size and configuration of the test cells do not represent any real livable building, and, therefore, do not manifest the actual interaction between the climatological parameters and a real building. This results in a greater impact for some of the variables (solar insolation will be more dominant in case of test cells) and lesser degree of interaction for others. Likewise, the location of the experiment (City of Las Vegas) and for that matter the overall climate type (hot-arid climate) also limit the generalizability of the findings. Nevertheless, well-conceived and properly calibrated analytical models should be able to predict the dependent variable fairly accurately as the independent variables changes.

3.2 Description of the test cells

The NEAT Lab test cells were built in 2004 as a design-build collaboration effort between UNLV School of Architecture undergraduate students and the NEAT Lab researchers. The roofpond (RP) and control (CC) test cells have an interior floor area of 29 ft^2 (2.69 m^2) and are identical in their construction, with the exception that the RP has a 9 inches (22.9 cm) deep roofpond over its ceiling. Both test cells have interior dimension of 4'-3" x 6'-10" x 8'-00" (130cm x 208cm x 244cm), with the larger facades facing north and south (see Fig. 9). The test cells are constructed with the traditional stick-frame method. The frames are made of wood-studs with plywood placed on both side of the frame (Fig. 10). Aluminum foil-covered polyisocyanurate rigid insulation (R=9.8 h-ft^2 °F / Btu or 1.73 m^2 °C / W) insulates the wall cavities (Figure 11 & Figure 12).

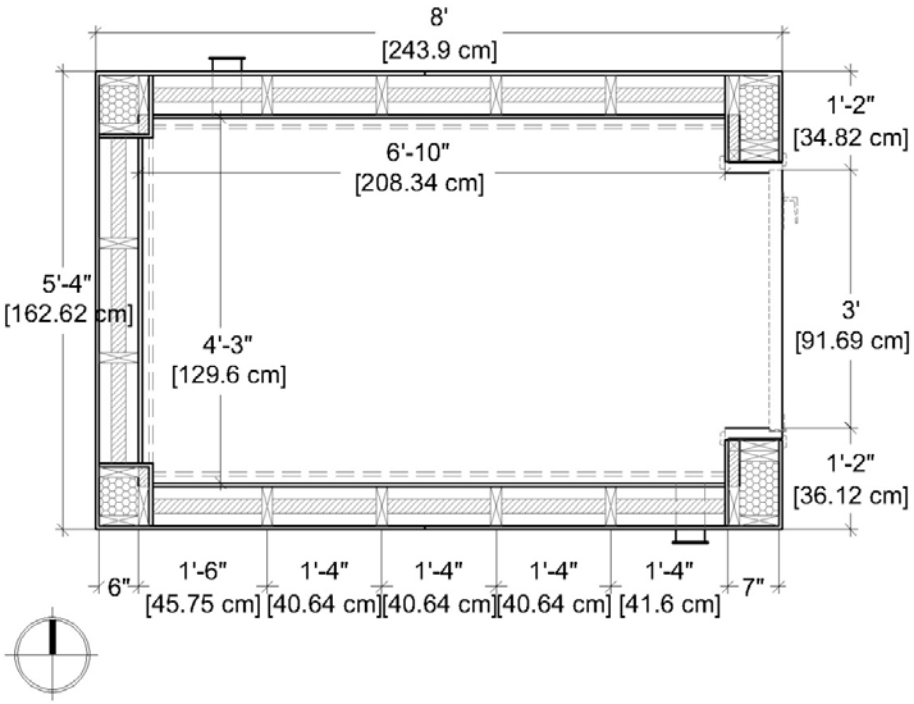

Figure 11: Basic floor plan of the test cells

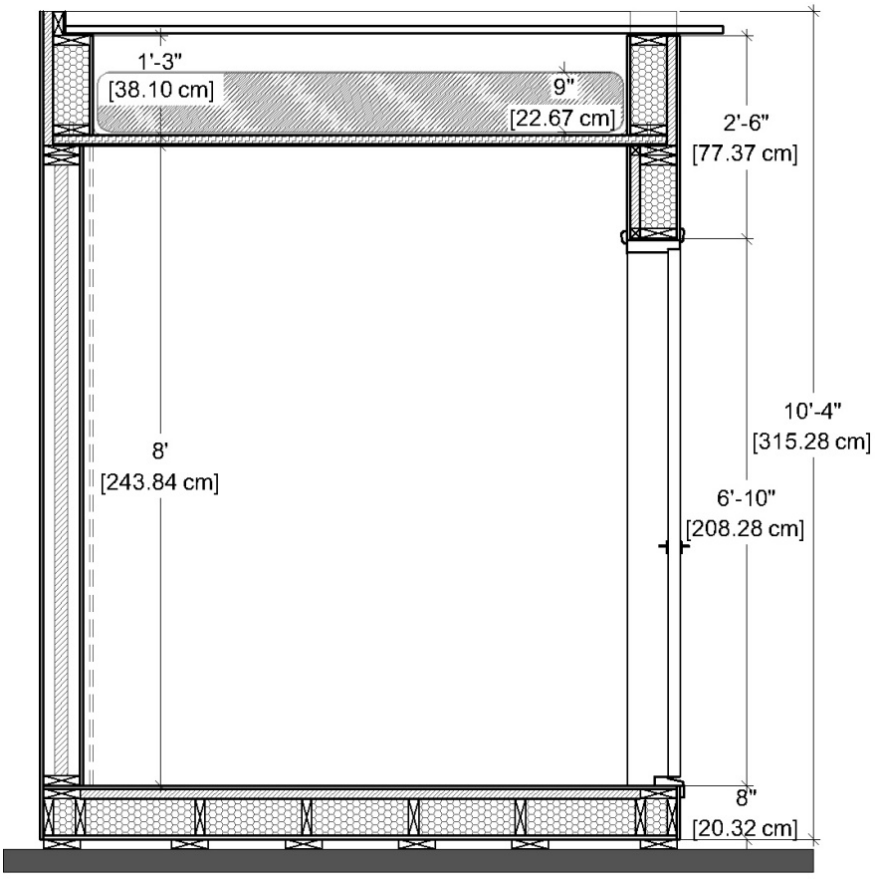

Figure 12: Longitudinal section of the test cells

Corrugated metal deck is used as structural ceiling. Sealed polyethylene bags filled with water are placed on top of the ceiling's EPDM liner (the CC does not have water bags). Standard automated garage doors provide the movable insulation for the roofpond (Figure 13). The Thermacore® garage doors used in this project have an R-value of 11.0 h-ft^2 °F/Btu (1.94 m^2 °C/W) and are suitable for roofpond applications in the US Southwest.

Figure 13: Standard garage door as the movable insulation

During the summer of 2009, the movable insulation panels were moved to cover the roofpond (or the ceiling, in the case of the CC) at 6:00 AM every day. The movable insulation panels of both test cells remained “closed” for 13 hours during the daytime to reduce heat gains from incident solar radiation and the hot outdoor air. The movable insulation panels were retracted in the evening at 7:00 PM, as the environment was cooler and could begin to absorb the heat gained by the roofpond (or the CC) throughout the day. Table 3 summarizes the operation of the test cell.

Table 2 summarizes the construction of the test cell. Details of construction properties of the test cells are included in the Appendix II.

Table 2. Physical properties of test cell construction

Test cell construction element	Symbol	Value	Unit	Value	Unit
Area of roof	A_{roof}	42.67	ft^2	3.96	m^2
Building floor area	A_{Floor}	29.04	ft^2	2.70	m^2
Ceiling area	$A_{ceiling}$	29.04	ft^2	2.70	m^2
Area of water surface (same as the ceiling area)	$A_{Water\ surface}$	29.04	ft^2	2.70	m^2
Area of north wall	A_{w_North}	64	ft^2	5.95	m^2
Area of south wall	A_{w_South}	64	ft^2	5.95	m^2
Area of west wall	A_{w_West}	29.04	ft^2	3.96	m^2
Area of east wall (including door)	A_{w_East}	29.04	ft^2	3.96	m^2
Area of door (on east wall)	A_{Door}	20.5	ft^2	1.90	m^2
Room air volume	V_{Air}	232.3	ft^3	6.58	m^3
Thickness of water mass	L_W	9	inch	0.23	m
U – value per area, north wall	h_{w_Nouth}	0.05	Btu/h ft^2 °F	0.30	W / m^2 °C
U – value per area, south wall	h_{w_South}	0.05	Btu/h ft^2 °F	0.30	W / m^2 °C
U – value per area, east wall	h_{w_East}	0.10	Btu/h ft^2 °F	0.55	W / m^2 °C
U – value per area, west wall	h_{w_West}	0.05	Btu/h ft^2 °F	0.30	W / m^2 °C
U – value per area, Floor	h_{Floor}	0.04	Btu/h ft^2 °F	0.22	W / m^2 °C
U – value per area, Roof insulation panel	h_{Roof}	0.09	Btu/h ft^2 °F	0.52	W / m^2 °C
U – value per area, Water mass (4.5 inch or 11.43 cm)	h_{Water_1}	0.61	Btu/h ft^2 °F	5.30	W / m^2 °C

This experimental research project uses a side-by-side comparison between a control cell (CC) and a roofpond (RP) to determine the thermal characteristics and benefits provided by the roofpond strategy. As mentioned earlier, both test cells have identical thermal properties, with the exception of the 9 inches (22.9 cm) deep water pond placed above the ceiling of the RP test cell. However, to develop the predictive formula, only the data from the RP cell are used.

Table 3. Operation of the test cell

Seasonal variation	Mode of operation	Diurnal changes	Insulation panel position
Winter months	Heating mode	Day-lit hours (7:00 AM - 3:59 PM)	Open
		Evening hours (4:00 PM - 6:59 AM)	Closed
Summer months	Cooling mode	Day-lit hours (6:00 AM - 6:59 PM)	Closed
		Evening hours (7:00 PM - 5:59 AM)	Open

3.3 Data collection

The equipment used to monitor the test cells was calibrated in a controlled environment prior to the beginning of each experimental phase to ensure that all the measurements are accurate and comparable. Each test cell was instrumented with four HOBO® H-8 RH/Temperature/2x External data loggers to measure indoor conditions and three HOBO® U-12 Outdoor/Industrial data loggers to record outdoor surface temperatures (Figure 14 & Figure 15). The internal sensors of the HOBO® H-8 RH/Temperature/2x External data loggers were used to measure the indoor air temperature and the relative humidity, while the external channels were used to measure the mean radiant temperature (using a black globe) and various indoor surface temperatures (Figure 16).

Figure 14: HOBO® H-8 RH/Temperature/2x External data logger

(Source: http://www.onsetcomp.com/d-image/large/Temp-RH-2x-External-Channel_H08-007-02.jpg)

Figure 15: HOBO® Outdoor/Industrial data logger

Figure 16: Monitoring the interior environmental conditions

Ambient air temperature, solar radiation and wind speed were recorded using a Davis WeatherLink weather station (Figure 17), placed near the test cells. Interior temperature was recorded using either standard 2-channel or 4-channel HOBO® H-8 RH/Temperature/2x External data logger at five minutes data recording interval.

Figure 17: HOBO® U30 Weather station

Data were measured and recorded in the data loggers and then downloaded from the data loggers into a computer every seven days due to the memory limitations of the data loggers. The battery level of the data loggers was also checked every week to make sure that data loggers were able to record data during the subsequent measurement period. Downloaded data were then organized in a standard spreadsheet template and scrutinized to check for inconsistency in the data set.

3.4 Transfer-function heat transfer model

To develop the transfer-function heat transfer model with time lag of one hour, hourly ambient air temperature data (T_a) for 14 days (From May 17-23 & June 9-15) were used. The effects of conduction, radiation and convection were taken into account using basic heat transfer equations.

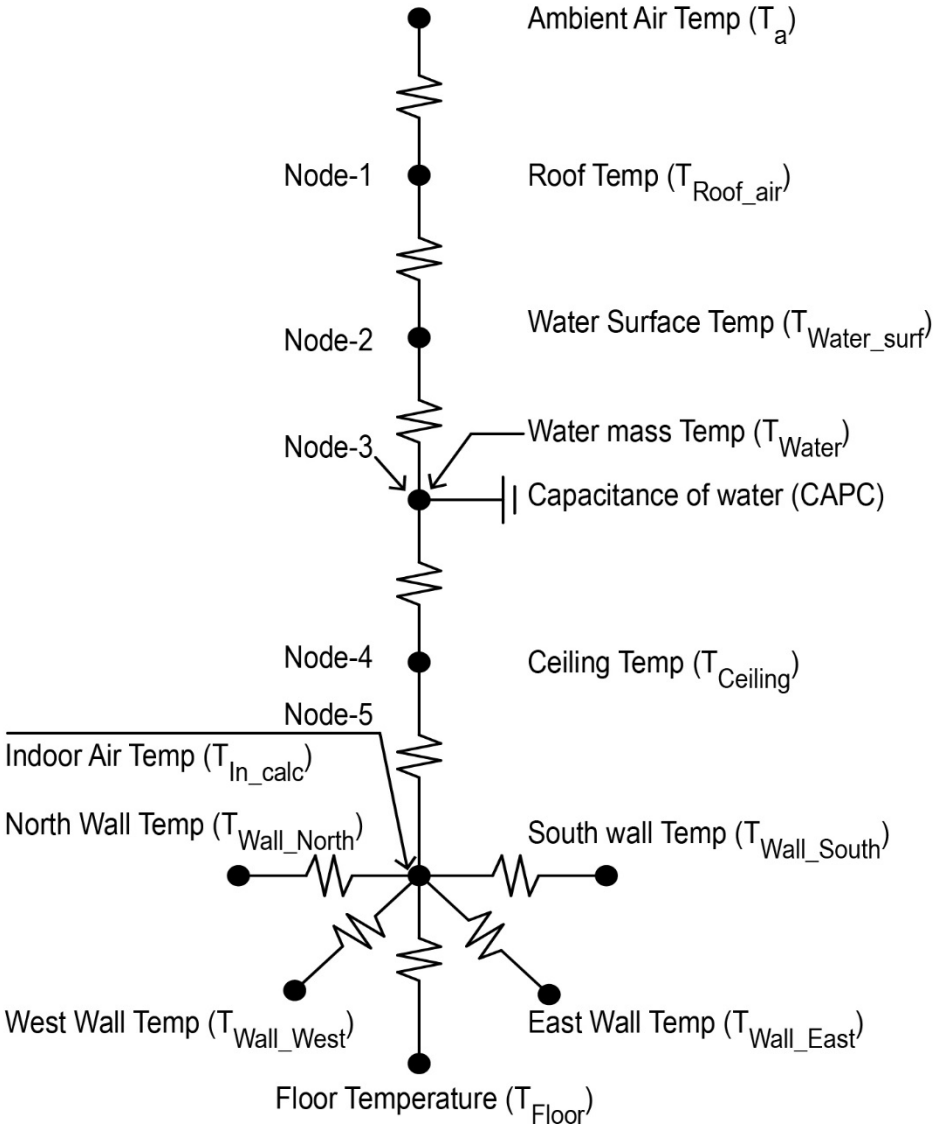

Figure 18: Thermal network (panel closed)

Figure 18 & Figure 19 present schematic diagrams of the thermal networks used to calculate the average indoor air temperature (T_{in}). Figure 18 represents the thermal network of the closed roofpond, whereas Figure 19 shows the thermal network of the roofpond when the panel is retracted.

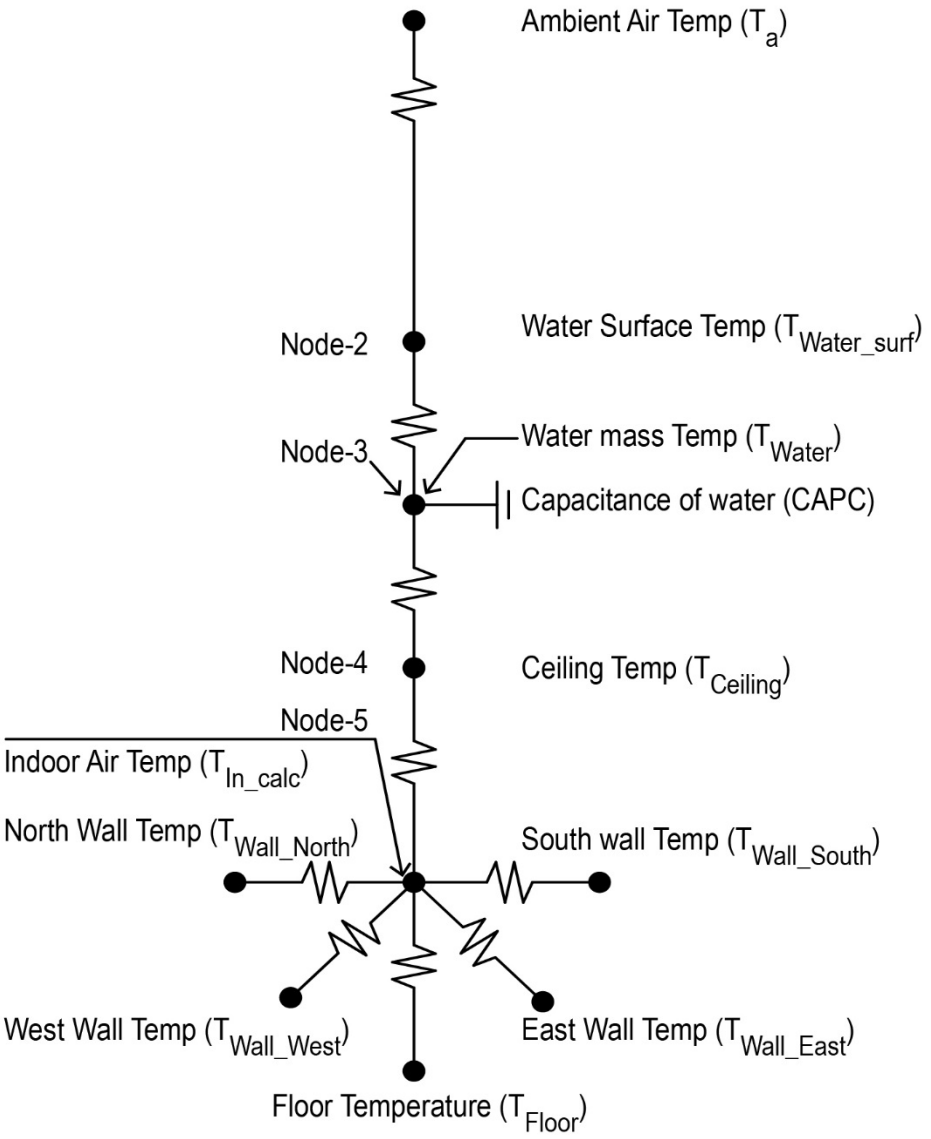

Figure 19: Thermal network (panel open)

To calculate conduction heat transfer, resistances of all the walls, roof and ground were calculated separately. A convective heat transfer coefficient (h_{con}) was also calculated to better represent the thermal network and to help determine the heat going in and coming out through the building. The heat absorbed by the roofpond from the test cell was of prime concern. Convective heat transfer coefficients for the roof assembly were found to have six different values depending on the operational mode of the panel, presented in Table 4.

To calculate the heat transfer between nodes, first the convective heat transfer coefficients (h_{con}) between different nodes were calculated. Convection heat transfer coefficient between the night sky and the open water mass (i.e. Insulation panel is open), $h_{Outside\_NO\ Panel}$ was calculated using the convection heat transfer coefficient of outside air (h_{Air_out}), coefficient for the convective heat loss/gain to the sky (h_{Con_sky}), and coefficient for the radiative heat loss/gain to the sky (h_{Rad_sky}).

Table 4. Direction of heat transfer through roof assembly

Position of Panel	Air space plane	Interior air film
Closed	Upward	Upward
Closed	Downward	Upward
Closed	Upward	Downward
Closed	Downward	Downward
Open	Exposed to outdoor	Downward
Open	Exposed to outdoor	Upward

Values for convection heat transfer coefficient of outside air, h_{Air_out}, are used from ASHRAE Handbook Fundamentals (SI) 2009 (ASHRAE, 2009) recommendation as listed below.

$h_{\mathrm{Air\_out}} = 22.00$ W / m^2 . °C, if the wind velocity is below 12 Km/h.

$h_{\mathrm{Air\_out}} = 34.00$ W / m^2 . °C, if the wind velocity is above 12 Km/h.

The coefficient for the convective heat loss/gain to the sky (h_{Con_sky}) can be calculated from the following equation (Hassid & Geros, 2006):

$$h_{\mathrm{Conv\_sky}} = 1.52 \times \Delta T^{1/3}$$

Where, ΔT is the absolute temperature difference between the ambient air temperature (T_a) and the temperature of the exposed roof surface (T_{Roof_air}), that is, $\Delta T = T_a - T_{Roof\_air}$.

Likewise, the coefficient for the radiative heat loss/gain to the sky (h_{Rad_sky}) can be calculated from the following equation (Kreider et al., 2010):

$$h_{\mathrm{Rad\_sky}} = \frac{4 \times \sigma \times T'^3}{\frac{1}{\varepsilon_{water}} + \frac{1}{\varepsilon_{sky}} - 1}$$

Where,

$\sigma = 5.67 * 10^{-8}$ W / m^2 . K^4 is Stefan-Boltzmann constant;

$T' = (T_a + T_{sky}) / 2$; average of ambient air temperature and sky temperature in Kelvin scale;

$\varepsilon_{water} = 0.93$; emissivity of water;

$\varepsilon_{sky} = 1.00$; emissivity of sky.

Once h_{Air_out}, h_{Con_sky}, and h_{Rad_sky} are calculated, the convection heat transfer coefficient between the night sky and the water mass, when the insulation panel is open, ($h_{Outside\_NO\ Panel}$) can be calculated using the following equation:

$$h_{\text{Outside\_NO Panel}} = \frac{1}{\frac{1}{h_{Air\_out}} + \frac{1}{h_{Conv\_sky}} + \frac{1}{h_{Rad\_Sky}}}$$

The garage door, acting as the insulation panel for the roofpond, has an insulation resistance of R=11.0 h-ft^2 °F/Btu (1.94 m^2 °C/W), thereby reducing the heat transferred between the water mass and the sky. This significantly changes the heat transfer coefficient between the sky and the enclosed water mass ($h_{Outside\_Panel}$). Since the resistance of the panel ($R_{Outside\_panel}$) is 11.0 ft^2 . F°. h / Btu:

$$h_{\text{Roof\_Panel}} = \frac{1}{11.0\ Btu\ /\ h.ft^2.°F} \times 5.68 = 0.516\ \text{W / m}^2\ .\ °\text{C}$$

$h_{Outside\_Panel}$ then can be calculated from the convection heat transfer coefficient of the roof insulation panel (h_{Roof_Panel}), which works in parallel with h_{Air_out}, h_{Con_sky} and h_{Rad_sky}, and therefore can be calculated using the following relationship:

$$h_{\text{Outside\_Panel}} = \frac{1}{\frac{1}{h_{Air\_out} + h_{Conv\_sky} + h_{Rad\_sky}} + \frac{1}{h_{Roof\_panel}}}$$

When the roof panel is retracted, there is a 6-inch air-gap between the roof panel and the water body. The air-gap itself acts as an insulation layer between the roof panel and the water body. The resistance of the air-gap changes according to the direction of heat flow. ASHRAE recommends R = 0.15 m^2 °C / W when heat is travelling upwards and R = 0.19 m^2 °C / W when heat is travelling downwards (ASHRAE, 2009). Therefore the convective heat transfer coefficient for the air-gap ($h_{Air\_in\_6"}$) is considered to be:

$$h_{\text{Air\_in\_6"}}\ (UP) = 6.667\ \text{W / m}^2.\ °\text{C}$$

$$h_{\text{Air\_in\_6"}}\ (DN) = 5.263\ \text{W / m}^2.\ °\text{C}$$

The convective heat transfer coefficient for the still air inside the test cell ($h_{Air\_in\_still}$) also depends on the direction of the heat flow. ASHRAE recommends the following values for $h_{Air\_in\_still}$ coefficient (ASHRAE, 2009):

$h_{\text{Air\_in\_still}}\ (UP) =\ 9.26$ W / m^2. °C

$h_{\text{Air\_in\_still}}\ (DN) =\ 6.13$ W / m^2. °C

The average temperature of the water mass (T_{Water}) is calculated in the middle of the water mass. Therefore, the 9-inch thick water mass is considered as two 4.5-inch thick water bodies.

$h_{\text{water\_1}} =\ 5.302$ W / m^2. °C, since water body is 4.5 inch deep

$h_{\text{water\_2}} =\ 5.302$ W / m^2. °C, since water body is 4.5 inch deep

The capacitance ($CAPC_{Water}$) of water is simply calculated multiplying the density of the water (ρ), by the specific heat of the water (C_p), and using the total volume of the water body.

$CAPC_{\text{Water}} =\ \rho\ \times\ \text{Cp\_water}\ \times\ \text{volume of the water} = 712.8$ Wh / °C where,

$\rho_{water} = 995.65$ kg / m^3.

$$\text{Cp}_{\text{water}} = \frac{4178.4\ \frac{J}{kg\ K}}{3600\ sec} = 1.161\frac{Wh}{kg\ K}$$

$V_{Water} = 2.698\ \times 0.229 = 0.617$ m^3

$A_{water\ surface} = 2.698$ m^2

$L_W = 0.229$ m (9 inch).

The convective heat transfer coefficients for all four walls and the floor have been calculated based on the material properties of the respective wall and floor construction (see, Appendix II). The convective heat transfer coefficients for the four walls and the floor are listed below.

$h_{\text{Wall\_North}} = 0.301$ W / m^2. °C

$h_{\text{Wall\_South}} = 0.301$ W / m^2. °C

$h_{\text{Wall\_East}} = 0.547$ W / m^2. °C

$h_{\text{Wall\_West}} = 0.301$ W / m^2. °C

$h_{\text{Floor}} = 0.222$ W / m^2. °C.

UA-values for the different nodes presented in Figure 18 & Figure 19 are calculated based on the above-mentioned equations. Calculated UA-values for one typical summer day are summarized in Table 5.

Table 5. Calculated UA-values at different nodes

Date	Time	$UA_{Outside\_Panel}$	$UA_{Air\_6"\_in}$	$UA_{Outside\_No\ Panel}$	$UA_{Effective}$	UA_{water_1}	UA_{water_2}	$UA_{Air\_in\_still}$	UA_{Air_infil}	UA_{Wall_North}	UA_{Wall_South}	UA_{Wall_East}	UA_{Wall_West}	UA_{Floor}
		(W/°C)	(W/°C)	(W/°C)	(W/°C)	(W/°C)	(W/°C)	(W/°C)	(W/°C)	(W/°C)	(W/°C)	(W/°C)	(W/°C)	(W/°C)
5/17	0:00	2.0	18.0	5.5	5.5	14.3	14.3	16.5	1.1	1.8	1.8	2.2	1.2	0.6
5/17	1:00	2.0	18.0	6.0	6.0	14.3	14.3	25.0	1.1	1.8	1.8	2.2	1.2	0.6
5/17	2:00	2.0	18.0	5.8	5.8	14.3	14.3	16.5	1.1	1.8	1.8	2.2	1.2	0.6
5/17	3:00	2.0	18.0	6.0	6.0	14.3	14.3	16.5	1.1	1.8	1.8	2.2	1.2	0.6
5/17	4:00	2.0	18.0	5.9	5.9	14.3	14.3	16.5	1.1	1.8	1.8	2.2	1.2	0.6
5/17	5:00	2.0	18.0	6.1	6.1	14.3	14.3	16.5	1.1	1.8	1.8	2.2	1.2	0.6
5/17	6:00	2.0	18.0	5.9	5.9	14.3	14.3	16.5	1.1	1.8	1.8	2.2	1.2	0.6
5/17	7:00	2.0	18.0	4.3	18.0	14.3	14.3	16.5	1.1	1.8	1.8	2.2	1.2	0.6
5/17	8:00	2.0	18.0	5.3	18.0	14.3	14.3	16.5	1.1	1.8	1.8	2.2	1.2	0.6
5/17	9:00	2.0	14.2	6.6	14.2	14.3	14.3	25.0	1.1	1.8	1.8	2.2	1.2	0.6
5/17	10:00	2.0	14.2	7.1	14.2	14.3	14.3	25.0	1.1	1.8	1.8	2.2	1.2	0.6
5/17	11:00	2.0	14.2	7.3	14.2	14.3	14.3	25.0	1.1	1.8	1.8	2.2	1.2	0.6
5/17	12:00	2.0	14.2	7.2	14.2	14.3	14.3	25.0	1.1	1.8	1.8	2.2	1.2	0.6
5/17	13:00	2.0	14.2	7.5	14.2	14.3	14.3	25.0	1.1	1.8	1.8	2.2	1.2	0.6
5/17	14:00	2.0	14.2	7.5	14.2	14.3	14.3	25.0	1.1	1.8	1.8	2.2	1.2	0.6
5/17	15:00	2.0	14.2	7.5	14.2	14.3	14.3	25.0	1.1	1.8	1.8	2.2	1.2	0.6
5/17	16:00	2.0	14.2	7.2	14.2	14.3	14.3	25.0	1.1	1.8	1.8	2.2	1.2	0.6
5/17	17:00	2.0	14.2	6.8	14.2	14.3	14.3	25.0	1.1	1.8	1.8	2.2	1.2	0.6
5/17	18:00	2.0	14.2	6.8	14.2	14.3	14.3	25.0	1.1	1.8	1.8	2.2	1.2	0.6
5/17	19:00	2.0	14.2	6.5	14.2	14.3	14.3	25.0	1.1	1.8	1.8	2.2	1.2	0.6
5/17	20:00	2.0	14.2	6.5	6.5	14.3	14.3	25.0	1.1	1.8	1.8	2.2	1.2	0.6
5/17	21:00	2.0	14.2	5.1	5.1	14.3	14.3	25.0	1.1	1.8	1.8	2.2	1.2	0.6
5/17	22:00	2.0	14.2	4.3	4.3	14.3	14.3	25.0	1.1	1.8	1.8	2.2	1.2	0.6
5/17	23:00	2.0	14.2	4.6	4.6	14.3	14.3	25.0	1.1	1.8	1.8	2.2	1.2	0.6

The transfer-function heat transfer model is used to calculate the temperature at each node, with a time lag of one hour (see Figure 18 & Figure 19). To calculate the temperature of any node, temperatures of all nodes interacting with that particular node are used. The equations used to calculate the temperature of the corresponding nodes are listed below.

Node-1:

$$T_{\text{Roof\_air}} = \frac{(UA_{Outside\_panel} \times T_a) + (UA_{Air\_6"\_in} \times T_{Water\_surf})}{UA_a + UA_{Water\_surf}}$$

Node-2:

$$T_{\text{Water\_surf}} = \frac{(UA_{Effective} \times T_{Effective}) + (UA_{Water\_1} \times T_{Water})}{UA_{Effective} + UA_{Water}}$$

$UA_{Effective}$ is the outdoor UA-value, acting on the water mass, based on the operational mode of the test cell. When the roof panels are retracted during day time (from 6:01 AM - 7:00 PM), the $UA_{Outside\_No\ Panel}$ will act as the effective UA-value for node-2. However, as the test cell switches to heating mode (i.e., panels are removed and the water mass is open to the sky from 7:00 PM - 5:59 AM), $UA_{Air\_6"\_in}$ will act as the effective UA-value for the node. Similarly, $T_{Effective}$ is the temperature based on the mode of operation of the test cell. From 6:00 AM - 6:59 PM T_{Roof_air}, which is significantly lower than the ambient temperature (T_a), will act as the effective temperature. During night time (from 7:00 PM - 5:59 AM), T_a becomes the effective temperature and interacts with node-2.

Node-3:

Current T_{water} value, *ie.* n=1, depends on the T_{water} value of the previous time step (n=0). Thus the following equation is used to calculate $T_{Water\ (n=1)}$:

$$T_{\text{Water}_{(n=1)}}$$

$$= \left[T_{Water_{(n=0)}}\right]$$

$$+ \left[\frac{\left\{UA_{Water_1} \times \left(T_{Water_{surf}} - T_{\text{Roof}_{\text{air}(n=0)}}\right)\right\} + \left\{UA_{Water_2} \times \left(T_{Ceiling} - T_{\text{Roof}_{\text{air}(n=0)}}\right)\right\}}{CAPC}\right]$$

Node-4:

$$T_{\text{Ceiling}} = \frac{(UA_{Water\_2} \times T_{Water}) + (UA_{Air\_in\_still} \times T_{In})}{UA_{Water\_2} + UA_{Air\_in\_still}}$$

Node-5:

$$T_{\text{in\_calc}} = \frac{\begin{array}{c}\left(UA_{Air\_in\_still} \times T_{Ceiling}\right) + \left(UA_{Air\_infill} \times T_a\right) + \\ \left(UA_{Wall\_north} \times T_{Wall\_north}\right) + \left(UA_{Wall\_south} \times T_{Wall\_south}\right) + \\ \left(UA_{Wall\_east} \times T_{Wall\_east}\right) + \left(UA_{Wall\_west} \times T_{Wall\_west}\right) + \left(UA_{Floor} \times T_{Floor}\right)\end{array}}{\begin{array}{c}[\, UA_{Air_{in_{still}}} + UA_{Air_{infill}} + UA_{Wall_{north}} + UA_{Wall_{south}} + \\ UA_{Wall\_east} + UA_{Wall\_west} + UA_{Floor}\,]\end{array}}$$

Since the surface temperature data already includes the effect of solar radiation on the various surfaces, Sol-Air temperature (T_{sol}) was not used in order to increase the accuracy of the calculated indoor air temperature (T_{in_calc}).

Table 6 summarizes the calculated temperatures at different nodes for one typical summer day.

Table 6. Calculated temperature at different nodes

Date	Time	T_a	T_{Roof_air}	$T_{Effective}$	T_{Water_surf}	T_{Water}	$T_{Ceiling}$	T_{Wall_North}	T_{Wall_South}	T_{Wall_East}	T_{Wall_West}	T_{Floor}	T_{in_calc}
		(°C)	(°C)	(°C)	(°C)	(°C)	(°C)	(°C)	(°C)	(°C)	(°C)	(°C)	(°C)
5/17	0:00	27.5	29.8	27.5	28.6	29.0	26.8	28.4	28.4	28.4	25.0	31.2	27.2
5/17	1:00	26.3	28.3	26.3	28.5	28.9	27.9	27.5	27.5	27.5	24.4	30.1	27.7
5/17	2:00	25.2	28.2	25.2	28.2	28.9	28.2	26.4	26.4	26.4	23.6	29.1	27.5
5/17	3:00	24.6	27.8	24.6	27.8	28.8	28.1	25.5	25.5	25.5	23.1	28.1	27.1
5/17	4:00	24.4	27.5	24.4	27.6	28.8	27.9	25.0	24.9	24.9	22.5	27.1	26.8
5/17	5:00	23.3	27.2	23.3	27.5	28.8	27.7	24.1	24.1	24.1	21.6	26.0	26.4
5/17	6:00	23.9	27.1	23.9	27.2	28.7	27.5	24.1	24.1	24.1	23.3	25.5	26.3
5/17	7:00	26.3	27.1	27.1	26.0	28.6	27.4	28.6	26.3	26.3	28.9	25.2	27.3
5/17	8:00	28.9	26.3	26.3	27.7	28.6	27.9	31.0	32.6	32.6	34.6	25.4	29.1
5/17	9:00	31.4	28.1	28.1	27.3	28.5	28.9	33.3	40.6	40.6	37.5	26.0	30.9
5/17	10:00	34.2	28.2	28.2	28.2	28.5	30.0	37.1	39.6	39.6	38.8	26.9	31.9
5/17	11:00	35.5	28.8	28.8	28.1	28.6	30.7	38.6	37.8	37.8	40.5	28.3	32.4
5/17	12:00	36.2	29.1	29.1	28.7	28.6	31.0	39.7	38.7	38.7	43.8	29.6	33.0
5/17	13:00	37.7	29.1	29.1	28.7	28.7	31.4	40.9	41.0	41.0	49.4	30.9	33.9
5/17	14:00	38.2	29.8	29.7	29.1	28.7	32.0	42.8	51.3	51.3	45.4	32.2	35.5
5/17	15:00	38.5	29.8	29.8	29.2	28.8	33.1	43.5	53.4	53.4	45.4	33.6	36.7
5/17	16:00	37.2	29.9	29.9	29.4	28.9	33.8	41.0	45.0	45.0	45.4	34.9	36.1
5/17	17:00	35.9	30.2	30.2	29.5	29.0	33.5	38.1	38.4	38.4	40.3	36.0	34.7
5/17	18:00	35.7	30.2	30.2	29.6	29.1	32.7	36.6	36.7	36.7	36.4	36.5	33.6
5/17	19:00	35.0	30.2	30.2	29.6	29.2	32.0	35.7	35.7	35.7	34.4	36.6	32.9
5/17	20:00	34.8	30.3	34.8	29.5	29.3	31.6	34.8	34.9	34.9	32.7	36.3	32.4
5/17	21:00	31.9	30.3	31.9	30.7	29.3	31.3	33.6	33.6	33.6	30.7	35.6	31.7
5/17	22:00	30.8	30.3	30.8	29.9	29.4	30.9	32.1	32.1	32.1	29.2	34.5	31.1
5/17	23:00	29.7	29.8	29.7	29.7	29.4	30.5	31.3	31.3	31.3	28.6	33.4	30.6

CHAPTER 4. ANALYSIS OF RESULTS

The first phase of the analysis used data collected from the roofpond test cell and implements unsteady-state thermal heat transfer principles to predict average interior air temperature. Measured data for 14 days (May 17-23, June 9-15) are used to develop the heat transfer model that can predict the average indoor air temperature. The predicted indoor air temperature (T_{in_calc}) was then compared against the measured indoor air temperature ($T_{in\_measured}$) to find the correlation and test for patterns in residuals (Figure 20).

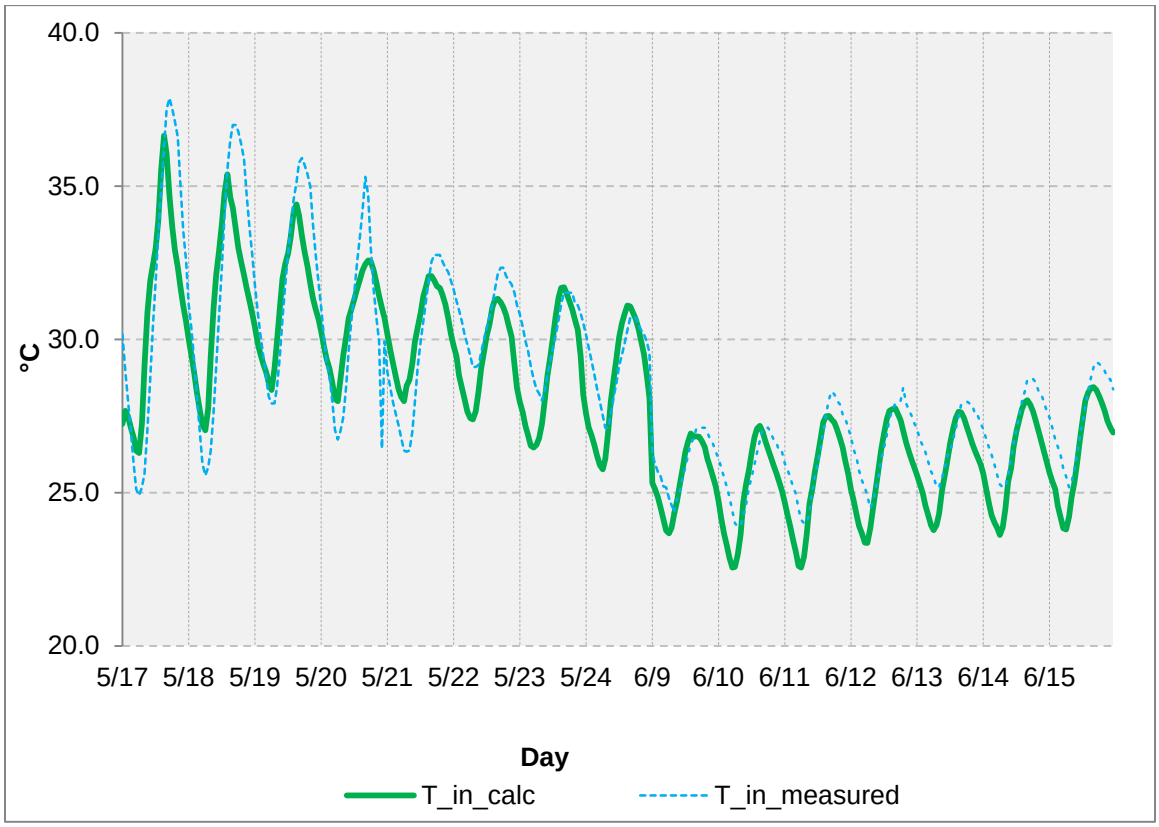

Figure 20: Simple correlation between the measured and the calculated temperature

Since patterns were observed in residuals, a time series model with Fourier series was used to de-trend the pattern. The implementation of Fourier series improves the

correlation and reduces the trend in residuals. Therefore, Auto Correlation Factor (ACF) and Partial Auto Correlation Factor (PACF) tests were used to select among Auto Regressive (AR), Moving Average (MA), and Auto Regressive Integrated Moving Average (ARIMA) models. The seasonal model was then summed with the AR / MA / ARIMA model to further reduce the seasonal trend. Once the best fit model was determined, it was tested against data from another summer month for validation.

4.1 Descriptive statistics:

Simple correlation analysis of the dependent versus the independent variable revealed a relative strong relationship. However, the relationship is not the strongest and can be attributed to experimental error. Relevant correlation parameters are listed in Table 7.

Table 7. Summary Statistics

	t_{in_calc}	$t_{in\_measured}$
	(°C)	(°C)
Average	27.8	28.7
Standard deviation	2.9	3.2
Minimum	20.4	23.9
Maximum	36.7	37.9
Range	16.3	14.0

4.2 Simple Regression:

The measured versus calculated indoor temperatures are plotted in Figure 20. A simple linear regression of the fitted model is expressed by the following equation:

$$t_{in\_measured} = 2.55611 + 0.930967 * t_{in\_calc}$$

Table 8. Simple Regression Coefficients

Parameter	Estimate	Standard Error	P-Value
Intercept	2.56	0.69	0.0002
Slope	0.93	0.02	0.0000

The P-value for both intercept and the slope is found to be statistically significant.

Table 9. Analysis of Simple Regression Variance

Source	Σ of Squares	P-Value
Model	2724.06	0.00
Residual	668.64	
Total (Corr.)	3392.7	

Correlation Coefficient = 0.896

R-squared = 80.29 %

Durbin-Watson statistic = 0.137

As expected, there is a statistically significant relationship between $t_{in\_measured}$ and t_{in_calc} at the 95.0% confidence level. The correlation coefficient is equal to 0.896058, indicating a moderately strong relationship between the variables (Figure 21). The lower value of the Durbin-Watson statistic tests also indicates the pattern in residuals. The residuals versus row order plot (Figure 22) reveals a cyclic pattern that is time (day) dependent, which indicates that inclusion of time variable (T) would yield a better relationship and might result in white noise.

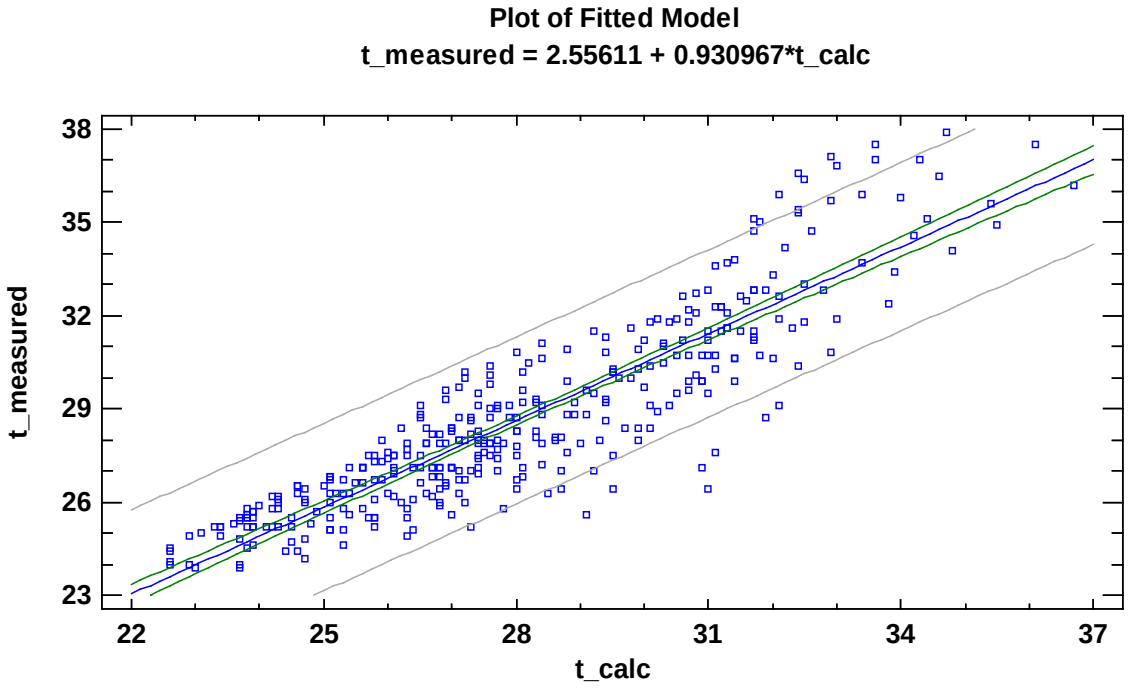

Figure 21: Linear correlation

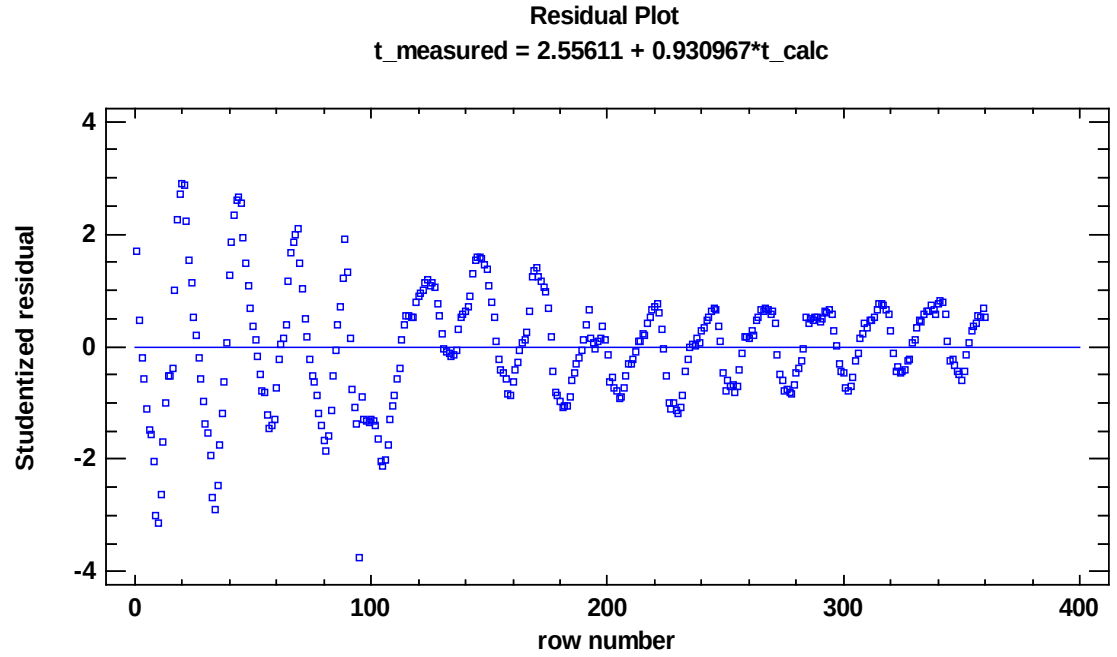

Figure 22: Model residuals

4.3 Time-series model:

The hourly outdoor temperature varies with the time of the day. Therefore, a frequency (ω) of 24 and an angular frequency of *[(2*pi)/24]*t* was used to capture the daily variation of the outdoor temperature. To that end, *sin((2*pi/24)t)*;*cos((2*pi/24)t)* and; *sin((2*pi/24)t)*cos((2*pi/24)t)* were introduced in the model. The measured versus the time-series predicted indoor temperature is plotted in Figure 23. A linear multiple regression yields the following relationship between the variables:

$t_{in\_measured} = 1.80566 + 0.961454 * t_{in\_calc} + 0.182754 * \sin(w_1 t) + 0.908795 * \cos(w_1 t) + 0.195899 * \sin(w_1 t) * \cos(w_1 t)$

Table 10. Time-series Model Coefficients

Parameter	Estimate	Standard error	P-Value
Constant	1.81	1.31	0.17
t_{in_calc}	0.96	0.05	0.00
sin(w_1t)	0.18	0.10	0.07
cos(w_1t)	0.91	0.05	0.00
sin(w_1t)*cos(w_1t)	0.20	0.08	0.01

Table 11. Analysis of Time-series Model Variance

Source	Σ of Squares	Df	P-Value
Model	263.23	4	0.00
Residual	20.46	163	
Total (Corr.)	283.69	167	

R-squared = 92.79 %

Standard Error of Est. = 0.354

Mean absolute error = 0.282

Durbin-Watson statistic = 0.321

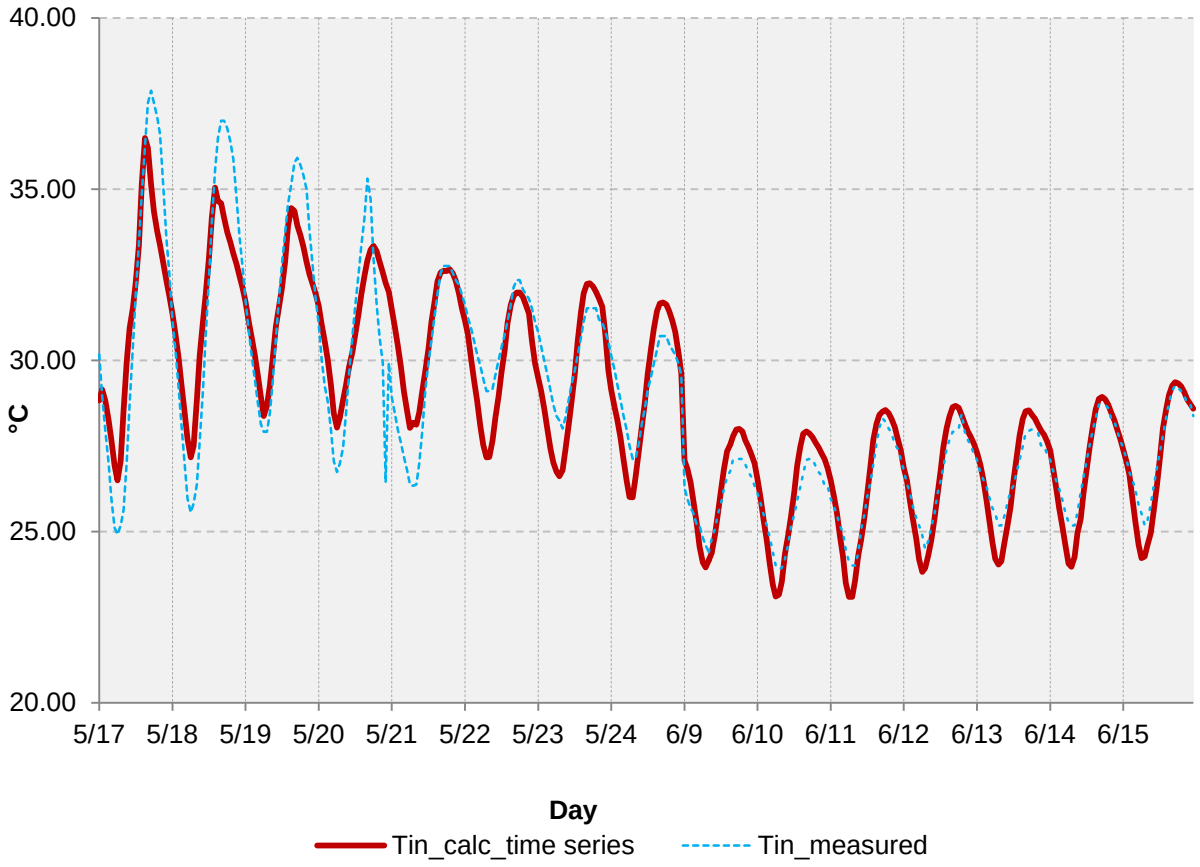

Figure 23: Simple correlation between the measured and time-series calculated temperature

Since the P-value in the ANOVA table is less than 0.05, there is a statistically significant relationship between the variables at the 95.0% confidence level (Figure 24). As expected, R^2 has improved by 13 percent, from 82% to 93%. However, a poor Durbin-Watson statistic represents the presence of cyclic residuals (Figure 25).

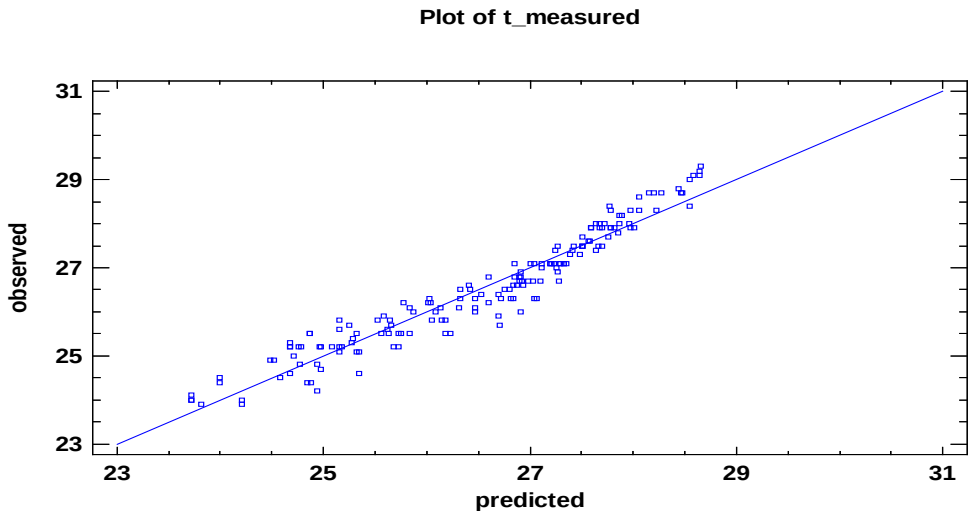

Figure 24: Time-series correlation

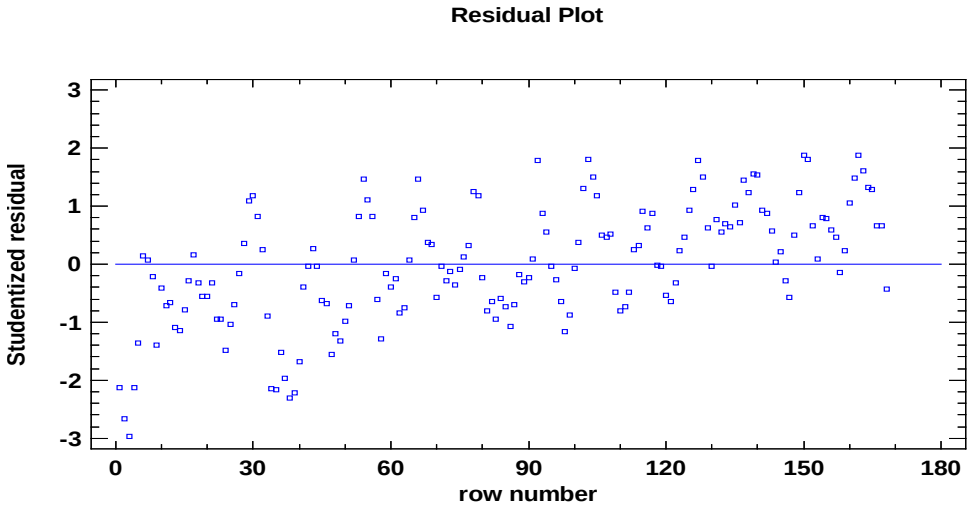

Figure 25: Model residuals from time-series correlation

The residuals are tested with an intention to develop ARIMA model, in any combination of AR, I, and MA to eliminate the cyclic behavior in residuals. In order to determine the appropriateness of ARIMA model, an ACF and PACF test was performed, yielding the following results shown in Figure 26 & Figure 27.

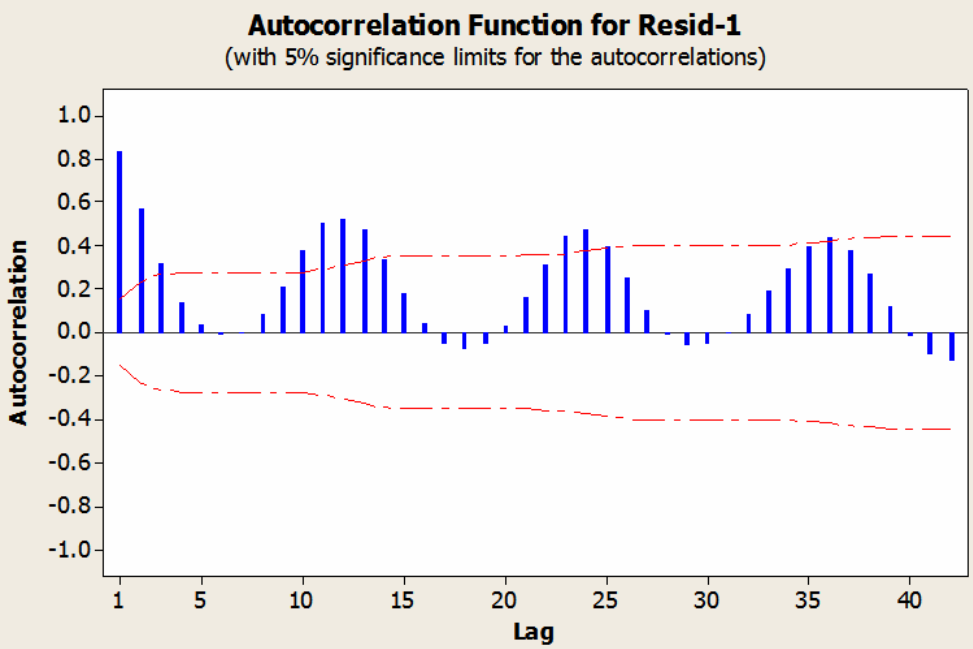

Figure 26: Autocorrelation of the residuals

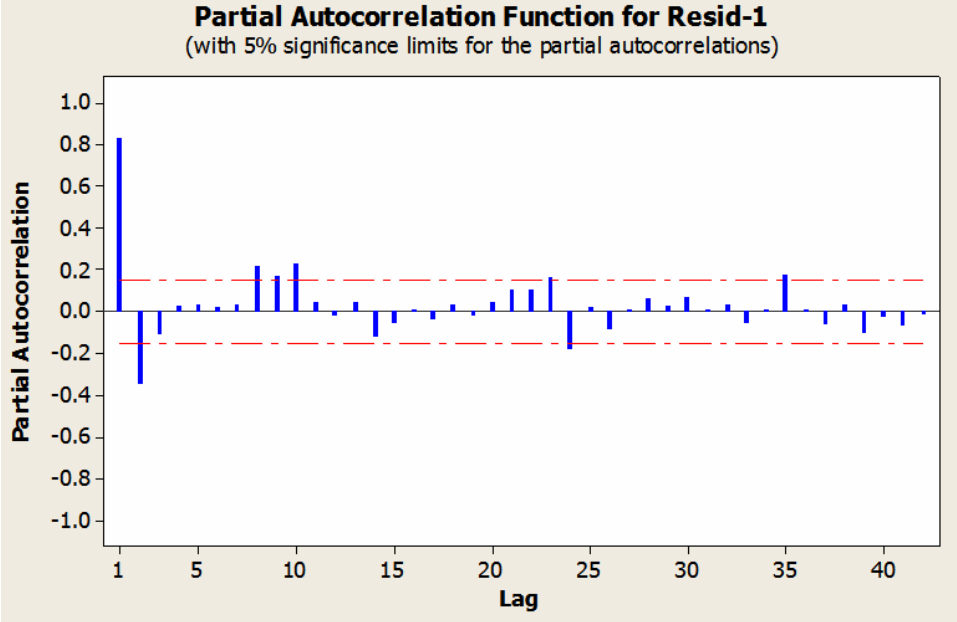

Figure 27: Partial Autocorrelation of the residuals

The ACF and PACF of the residuals from the time-series model reveals that an AR(2) model will best fit the data. Nonetheless, all three AR(1), AR(2), and ARIMA(1,0,1) model were developed to compare the performance of each of them.

4.4 Seasonal + AR (1) model:

The following relationship was calculated from AR (1) model:

$$Z_t = \phi_1 Z_{t-1} + a_t = 0.8521^* Z_{t-1} - 0.00406$$

Table 12. Seasonal + AR (1) model Coefficients

Type	Coefficient	Standard Error Coefficient	P-Value
AR (1)	0.85	0. 04	0.00
Constant	- 0.004	0. 014	0.78
Mean	- 0.03	0. 098	

However, the constant is found to be insignificant and therefore excluded from the time-series AR (1) model. The model thus yields as the following:

AR (1): $t_{in\_measured} = 1.80566 + 0.961454 * t_{in\_calc} + 0.182754 * \sin(w_1 t) + 0.908795 * \cos(w_1 t) + 0.195899 * \sin(w_1 t) * \cos(w_1 t) + 0.8521^* Z_{t-1} - 0.00406$

This model yields a higher R^2 with a significantly higher Durbin-Watson statistic. The residuals also lacks in cyclic pattern (Figure 28 & Figure 29).

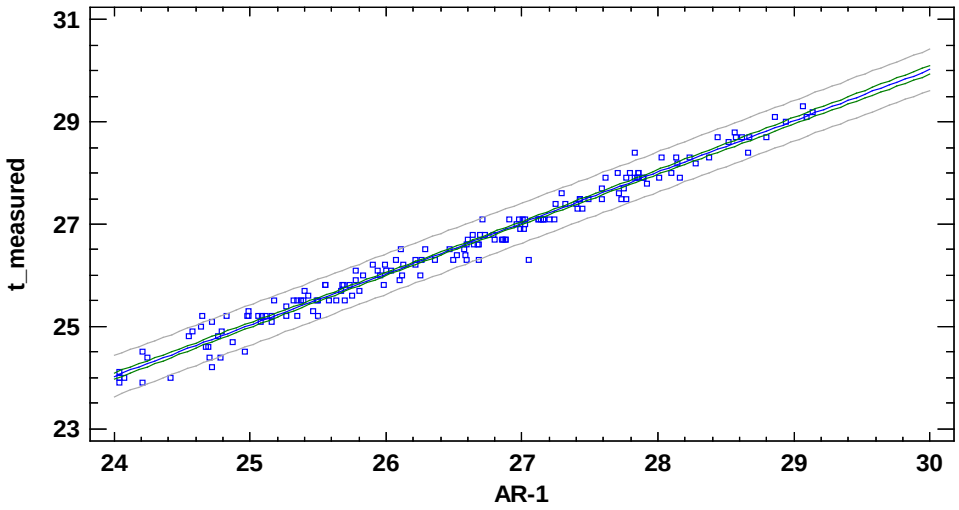

Figure 28: AR (1) correlation

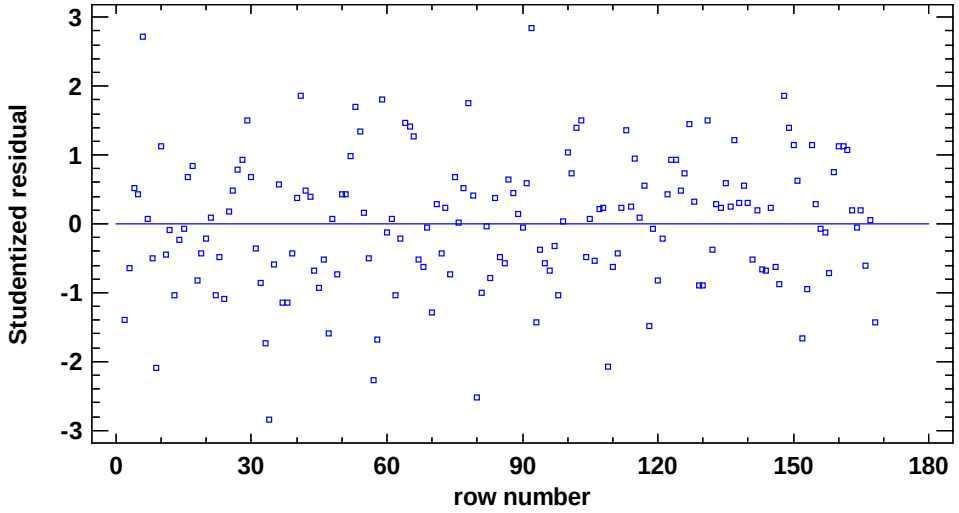

Figure 29: AR (1) model residuals

4.5 Seasonal + AR (2) model:

The following relationship was calculated from AR (1) model:

$Z_t = \phi_1 Z_{t-1} + \phi_2 Z_{t-2} + a_t = 1.1417 * Z_{t-1} - 0.3562 * Z_{t-2} - 0.00989$

Table 13. Seasonal + AR (2) model Coefficients

Type	Coefficient	Standard Error Coefficient	P-Value
AR (1)	1.14	0. 07	0.00
AR (2)	-0.36	0.07	0.00
Constant	-0.002	0.01	0.88
Mean	-0.01	0.06	

The constant is found to be statistically insignificant and, therefore, is not included in the time-series AR (2) model. The model thus yields as the following:

AR (2): $t_{in\_measured}$= 1.80566 + 0.961454 * t_{in_calc} + 0.182754 * sin(w_1t) + 0.908795 * cos(w_1t) + 0.195899 * sin(w_1t) * cos(w_1t) + 1.1417 * Z_{t-1} - 0.3562 * Z_{t-2}

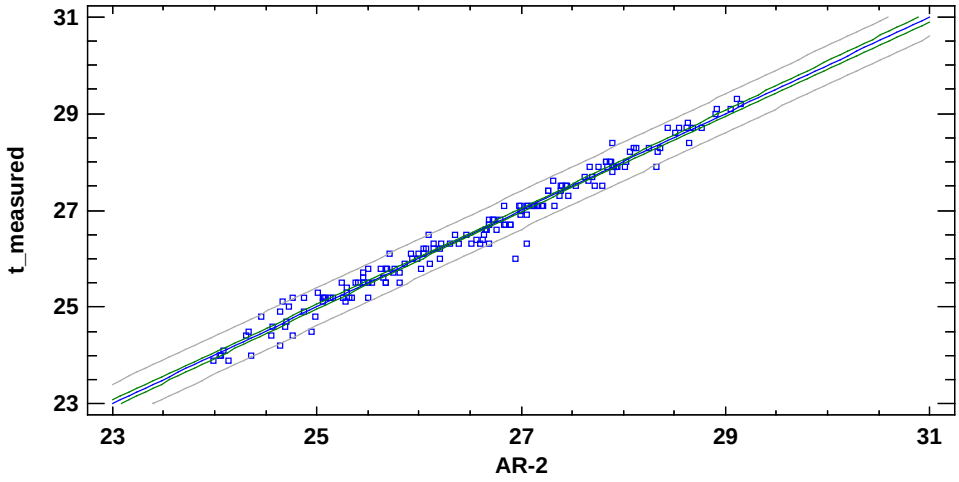

Figure 30: AR (2) correlation

The AR(2) model yields a R^2= 97.69% with an improved Durbin-Watson statistic (1.741). The residuals plot shows mostly white noise and loosely cyclic patterns (Figure 30 & Figure 31).

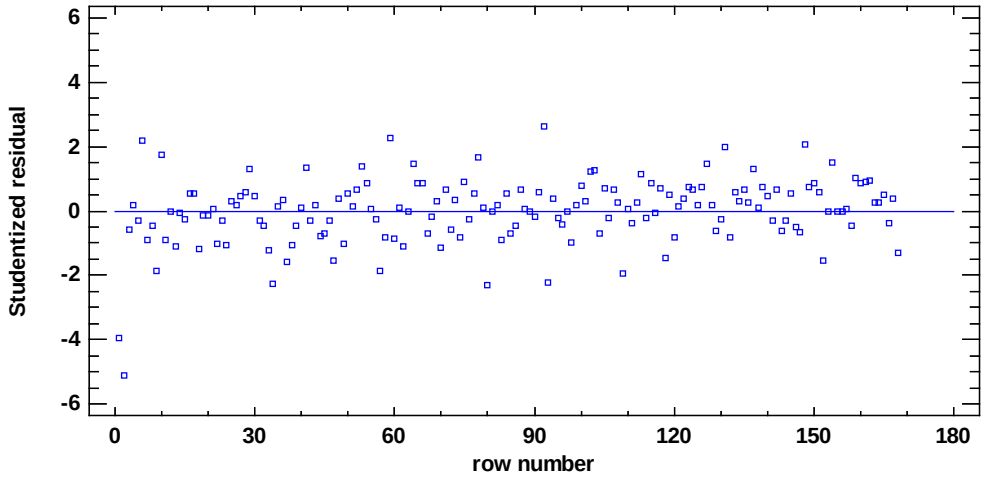

Figure 31: AR (2) model residuals

4.6 Seasonal + ARIMA (1,0,1) Model:

The following relationship was calculated from ARIMA (1,0,1) model:

$Z_t = \phi_1 Z_{t-1} + \omega_1 Z_{t-1} + a_t = 0.7709 * Z_{t-1} - 0.3084 * Z_{t-1} - 0.00410$

Table 14. Seasonal + ARIMA (1,0,1) model Coefficients

Type	Coefficient	Standard Error Coefficient	P-Value
AR (1)	0.77	0. 06	0.00
MA (1)	-0.31	0.09	0.00

The constant is found to be insignificant and is not included in the time-series ARIMA (1,0,1) model. The model thus yields as the following:

ARIMA (1,0,1): $t_{in\_measured}$= 1.80566 + 0.961454 * t_{in_calc} + 0.182754 * sin(w_1t) + 0.908795 * cos(w_1t) + 0.195899 * sin(w_1t) * cos(w_1t) + 0.7709 * Z_{t-1} -0.3084 * Z_{t-2}

The ARIMA (1,0,1) model yields somewhat smaller R^2 (96.26 %) with a significantly decreased Durbin-Watson statistic (0.8339). The residuals plot reveals the cyclic patterns (Figure 32 & Figure 33).

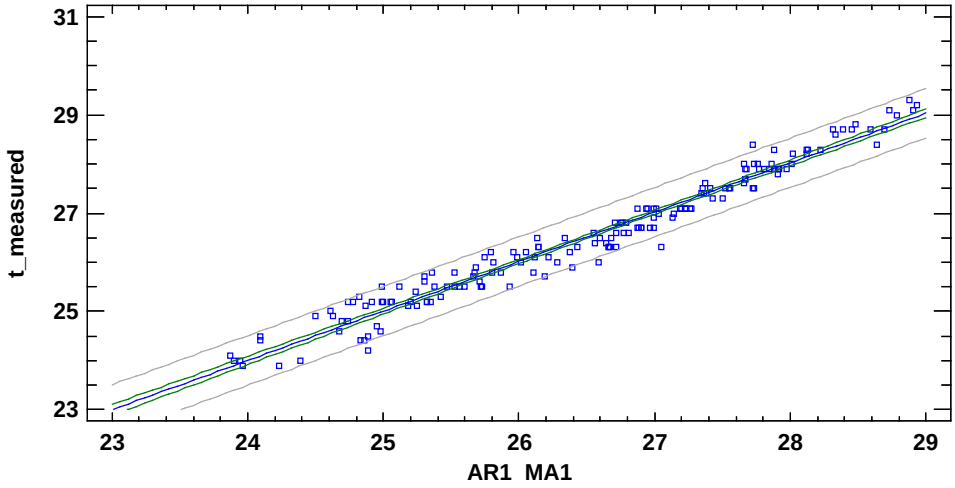

Figure 32: ARIMA (1,0,1) correlation

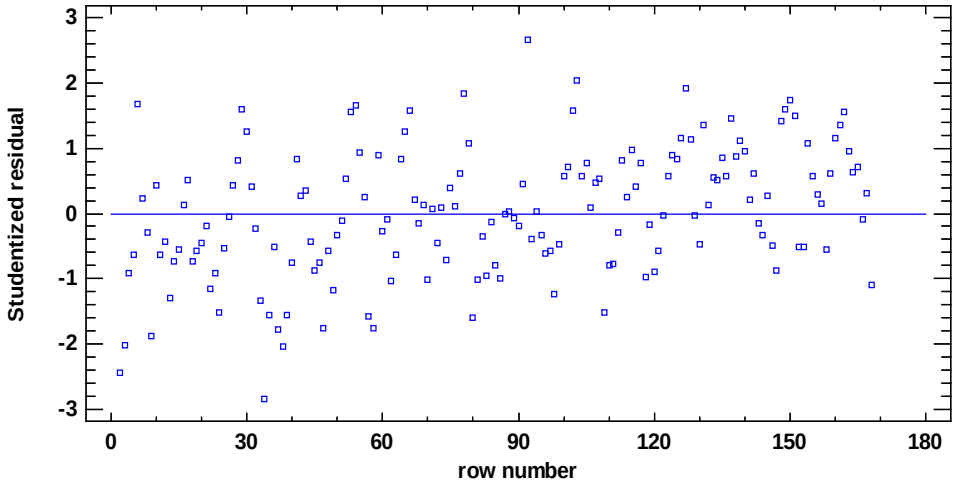

Figure 33: ARIMA (1,0,1) model residuals

4.7 Comparison of the different models

The three models, Seasonal + AR (1), Seasonal + AR (2), and Seasonal + ARIMA (1,0,1), are listed below:

Seasonal + AR (1) Model: $t_{in\_measured}$ = 1.80566 + 0.961454 * $_{tin\_calc}$ + 0.182754 * sin(w_1t) + 0.908795 * cos(w_1t) + 0.195899 * sin(w_1t) * cos(w_1t) + $\phi_1 Z_{t-1} + a_t = 0.8521* Z_{t-1}$

Seasonal + AR (2) Model: $t_{in\_measured}$= 1.80566 + 0.961454 * t_{in_calc} + 0.182754 * sin(w_1t) + 0.908795 * cos(w_1t) + 0.195899 * sin(w_1t) * cos(w_1t) + 1.1417 * Z_{T-1} - 0.3562 * Z_{T-2}

Seasonal + ARIMA (1,0,1) Model: $t_{in\_measured}$= 1.80566 + 0.961454 * t_{in_calc} + 0.182754 * sin(w_1t) + 0.908795 * cos(w_1t) + 0.195899 * sin(w_1t) * cos(w_1t) + 0.7709 * Z_{T-1} -0.3084 * Z_{T-2}

A comparison of the three models is consistent with the findings from the ACF and PACF test, and yields the Seasonal + AR(2) model as the best fit model. Therefore, the Seasonal + AR(2) model is used to predict the indoor air temperature of the roofpond test cell and is used for validation.

Table 15. Comparison of the three models

	Seasonal + AR (1)	Seasonal + AR (2)	Seasonal + ARIMA (1,0,1)
R-squared (%)	97.70	97.69	96.26
Mean absolute error	0.15	0.14	0.20
Durbin-Watson statistic	1.34	1.74	0.83

4.8 Validation of the model

The Seasonal + AR (2) model $t_{in\_measured} = 1.80566 + 0.961454 * t_{in\_calc} + 0.182754 * sin(w_1 t) + 0.908795 * cos(w_1 t) + 0.195899 * sin(w_1 t) * cos(w_1 t) + 1.1417 * Z_{t-1} - 0.3562 * Z_{t-2}$ model is used to predict the indoor hourly air temperature for 10 days (September 1st to 10th). Figure 34 shows the measured vs. predicted indoor temperature.

A linear regression between predicted and measured daily indoor average temperature yields the following test statistics: R-squared = 97.56%, Mean absolute error = 0.444, Durbin-Watson statistic = 0.323. Though the R^2 is higher and the RMSE is acceptably lower, the Durbin-Watson statistic is considerably lower, which indicates presence of pattern in residuals.

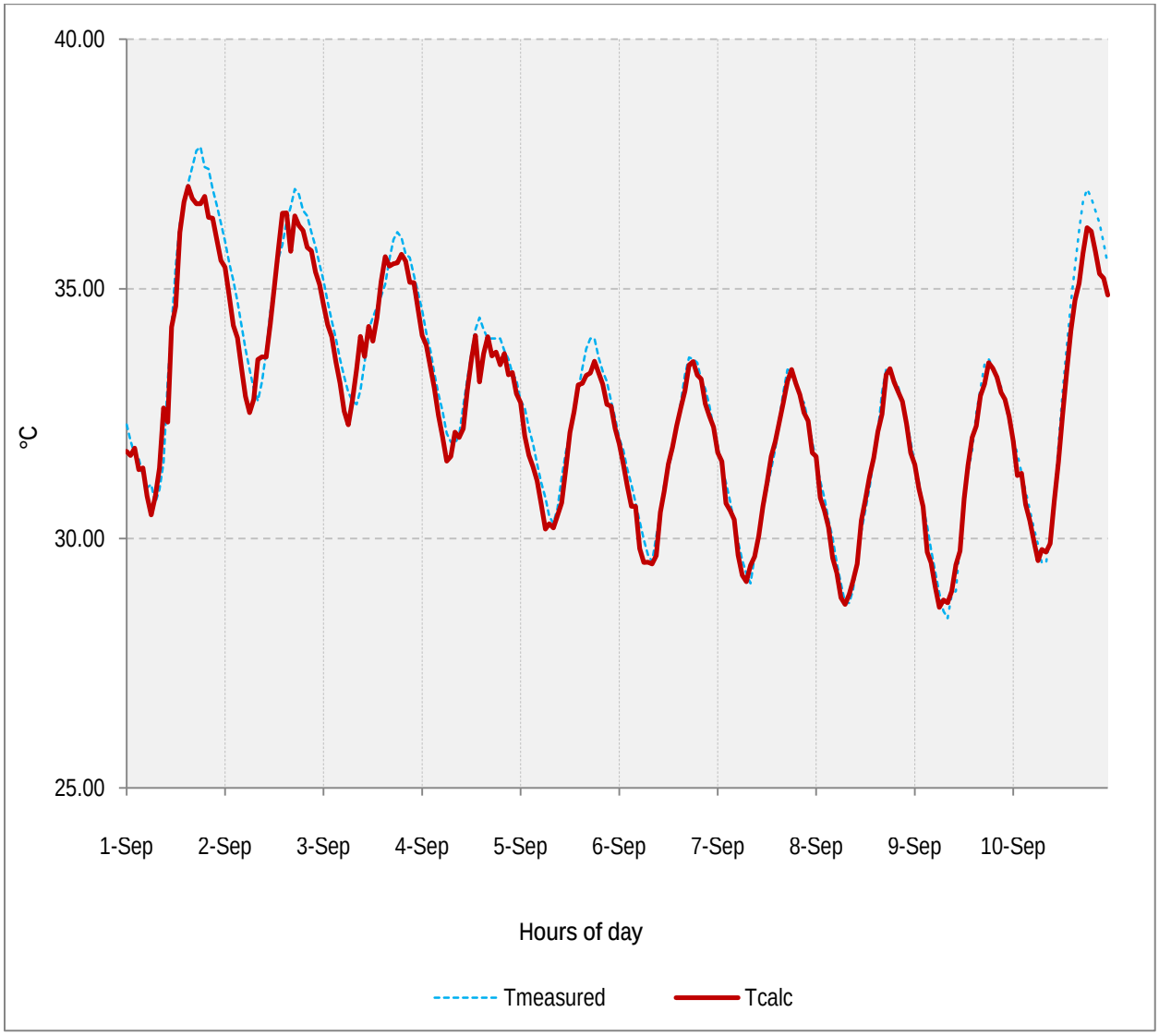

Figure 34: Measured and calculated time-series temperature

The plot of the residuals also reveals a trend (Figure 35). However, the pattern of the residuals is too large to be considered a daily cycle. Though it is not clear from the test, the pattern might be attributed to seasonal variation. Using a larger data set would be helpful in explaining as well as de-trending the pattern.

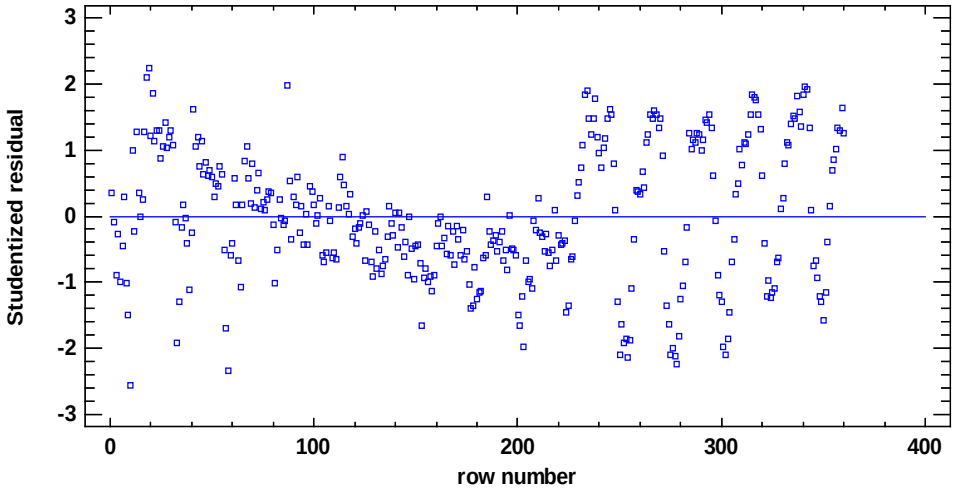

Figure 35: Validation model residuals

CHAPTER 5. CONCLUSIONS

5.1 Summary of the findings

A thermal network model that utilizes the unsteady state transfer-function method mimics the heat transfer in a dry roofpond building and can predict the indoor air temperature fairly accurately. This model incorporates an analysis of heat gain/loss mechanism and is more generalizable. The transfer-function unsteady state model requires the measured temperatures of the exterior surfaces including walls, ceiling and floor, as well as the ambient air temperature.

Indoor air temperature of a passive building, such as roofpond building is directly influenced by the outdoor air temperature; hence, it has a strong correlation with the time of day. However, the relationship is not as strong as it was hypothesized and a linear regression between calculated and measured temperatures only yields a moderately strong relationship while depict a strong daily pattern in their residuals. A time-series model on the other hand is found to be an appropriate model to address the cyclic pattern present in the difference between calculated and measured indoor air temperatures. The time-series model also helped to improve the correlation between the two variables significantly and, more importantly, it helped de-trended patterns in residuals. However, given that the time-series model still showed a pattern, an ARIMA model is used to further de-trend the residual patterns.

An ACF and PACF test demonstrated that a Seasonal + AR(2) model improves the residuals (*i.e.*, the patterns are significantly de-trended). The test statistics of Seasonal + AR(1), Seasonal + AR(2), and Seasonal + ARIMA(1,0,1) also revealed the appropriateness of using an Seasonal + AR(2) model and supported the test findings from ACF and PACF.

The same model was then tested for another 10 days in August (Fig. 26). The correlation is found to be acceptably higher with residuals revealing a pattern different than the previously identified daily change. This new trend might be due to seasonal variation which could be de-trended with a larger data set that encompasses the seasonal variation in temperature data.

The validated model can be used to predict indoor air temperature for a dry roofpond building, especially during the early design phase to evaluate as well as improve performance the proposed design. The simple spreadsheet used in this research to calculate the indoor air temperature is rather easy to use and can be modified to represent the thermal characteristics of most of the single story buildings in the United States Southwest. The change in the number of exterior surfaces can be easily accommodated in the model simply by adding or deducting nodes from the thermal model shown in this thesis. Likewise, once the model is modified and calibrated with any existing roofpond buildings, it can be used by the users to predict the indoor air temperature.

5.2 Benefits of using a hybrid model

Most of the earlier researches on roofpond system focused on developing accurate physical model for roofpond systems. These models extensively used first order heat transfer equations to predict the performance of roofpond system. Nevertheless, lack of availability of precise instruments as well as lower computational power made it difficult to accurately measure and compute the indoor air temperatures in a roofpond building. On the other hand, empirical models were able to accurately predict indoor air temperature for a roofpond building using minimal climatic information. However, these

empirical models with their higher accuracy level, are incapable of addressing changes in system configuration as well as climatic parameters.

Since the hybrid model proposed in this thesis is primarily developed based on the first order heat transfer equations and then fine-tuned empirically, the model incorporates the flexibility of a physical model and the accuracy of an empirical model. The model took into consideration the effect of whole building heat transfer mechanism and can easily be modified for different building configuration, construction characteristics, and weather conditions. Fine-tuning the model empirically ensures that the model will predict the indoor air temperature of a roofpond building more accurately.

5.3 Recommendations

The proposed predictive model was expected to be general and residuals were expected to be free of any patterns, *i.e.* residuals should be only white-noise. As mentioned earlier, one of the significant drawbacks of the proposed predictive model is the presence of patterns in residuals. Though the model yields significantly higher R^2 (97.56%) and lower RMSE (0.44), the Durbin-Watson statistic is considerably lower. Therefore, it is recommended that the model is further tested to de-trend residuals.

To develop the transfer-function unsteady state model surface air temperature was used instead of Sol-Air temperature (T_{sol}), in order to increase the accuracy of the model. However, the model can be further simplified by employing Sol-Air temperature (T_{sol}) and the solar radiation data from the nearby weather station as there is no need to measure surface temperature of all exterior surfaces. Though the prediction might be less accurate, the model is more general in nature.

As the model is based on basic heat-transfer equations, it is expected that the model will perform with same accuracy regardless of the climatic zone. However, it is recommended that the model should be tested for other climate zones as well for accuracy since the model is developed using the weather characteristics of hot-arid climate of the U. S. Southwest. Likewise, the model should be tested for a building with different construction properties in order to verify accuracy.

The validated model can also be used to develop simple computer programs or smart-phone apps with simplified front end user interface that will help the building users to predict the indoor air temperature based on the weather forecast and, thus, to adjust their building operation schedule to decrease the cooling load. However, since residential system loads are primarily imposed by heat loss or gain through structural components, and by air leakage or controlled ventilation the estimation might not be the most accurate prediction.

The proposed model is developed utilizing characteristics of a dry roofpond system that uses convective and radiative cooling. Wet roofpond buildings function differently and use evaporative cooling to increase the cooling performance. In fact, dry roofponds alone cannot provide the necessary cooling in hot-arid climate of the U. S. Southwest; wet roofponds are more effective in providing cooling in this region. It will be extremely useful to further explore the roofpond research utilizing the proposed method of this research but for a wet roofpond system. The test cells at the NEAT Lab can be easily converted to a wet roofpond system and used for data collection. The research presented in this thesis can be used as a reference for the future roofpond research.

APPENDIX I: NOMENCLATURE

$A_{ceiling}$	-	Area of the ceiling
A_{Door}	-	Area of the door on east wall
A_{Floor}	-	Test cell floor area
A_{roof}	-	Test cell roof area
$A_{Water\ surface}$	-	Area of the water surface
A_{w_East}	-	Area of the east wall
A_{w_North}	-	Area of the north wall
A_{w_South}	-	Area of the south wall
A_{w_West}	-	Area of the west wall
ACH	-	Air changes (per hour)
C_{p_air}	-	Specific heat of air
C_{p_water}	-	Specific heat of water
$CAPC_{water}$	-	Capacitance of water
$h_{Air\_in\_6"}$ (UP)	-	Upward convective heat transfer coefficient of still air between the roof panel and water mass
$h_{Air\_in\_6"}$ (DN)	-	Downward convective heat transfer coefficient of still air between the roof panel and water mass
$h_{Air\_in\_6"}$	-	Convective heat transfer coefficient of still air between the roof panel and water mass
$h_{Air\_in\_still}$ (UP)	-	Upward convective heat transfer coefficient of still air beneath the ceiling

$h_{Air\_in\_still}$ (DN) - Downward convective heat transfer coefficient of still air beneath the ceiling

$h_{Air\_in\_still}$ - Convective heat transfer coefficient of still air beneath the ceiling

$h_{Air\_out\ (24\ Km/h)}$ - Convective heat transfer coefficient of outside air when air velocity is over 24 Km/h

$h_{Air\_out\ (12\ Km/h)}$ - Convective heat transfer coefficient of outside air when air velocity is over 12 Km/h

h_{conv_sky} - Convective heat transfer coefficient to the sky

h_{Floor} - Convective heat transfer coefficient of floor

$h_{Outside\_NO\ Panel}$ - Combined convective heat transfer coefficient between night sky and water mass, without the roof insulation panel

$h_{Outside\_Panel}$ - Combined convective heat transfer coefficient between sky and water mass, with the roof insulation panel

h_{Roof_panel} - Convective heat transfer coefficient of the roof panel

h_{water_1} - Convective heat transfer coefficient of upper half of the water mass

h_{water_2} - Convective heat transfer coefficient of lower half of the water mass

h_{rad_sky} - Radiative heat transfer coefficient to the sky

h_{Wall_North} - Convective heat transfer coefficient of north wall

h_{Wall_South} - Convective heat transfer coefficient of south wall

h_{Wall_East} - Convective heat transfer coefficient of east wall

h_{Wall_West} - Convective heat transfer coefficient of west wall

L_W	-	Thickness of water mass
m_{air}	-	Mass flow rate of air
T_a	-	Ambient air temperature
$T_{Ceiling}$	-	Calculated ceiling temperature
$T_{Effective}$	-	Effective temperature between T_a and T_{Roof_air} based on operational mode of the roof insulation panel
T_{in_calc}	-	Calculated indoor air temperature
$T_{in\_measured}$	-	Measured indoor air temperature
T_{Roof_air}	-	Calculated insulation roof panel surface temperature
T_{sol}	-	Sol-air temperature
T_{Wall_East}	-	Measured surface temperature of the east wall
T_{Wall_North}	-	Measured surface temperature of the north wall
T_{Wall_South}	-	Measured surface temperature of the south wall
T_{Wall_West}	-	Measured surface temperature of the west wall
T_{water}	-	Calculated temperature of the of the water mass
$T_{Water\ (n=0)}$	-	Temperature of the water mass at previous time step
$T_{Water\ (n=1)}$	-	Temperature of the water mass at current time step
T_{Water_surf}	-	Surface temperature of the water mass
$UA_{Air\_in\_6"}$	-	U-value of the 6" air between insulation roof panel and water mass
$UA_{Air\_in\_still}$	-	U-value of the of still air beneath the ceiling
UA_{Air_infil}	-	U-value of the air infiltration
$UA_{Effective}$	-	U-value between $UA_{Air\_6"\_in}$ and $UA_{Outside\_NO\ Panel}$ based on

operational mode of the roof insulation panel

$UA_{Outside\_Panel}$	-	U-value of the roof with panel
$UA_{Outside\_No\ Panel}$	-	U-value of the roof without panel
UA_{water_1}	-	U-value of upper half of the water mass
UA_{water_2}	-	U-value of lower half of the water mass
UA_{Wall_East}	-	U-value of the east wall
UA_{Wall_North}	-	U-value of the north wall
UA_{Wall_South}	-	U-value of the south wall
UA_{Wall_West}	-	U-value of the west wall
V_{air}	-	Room air volume
$V_{test\text{-}cell}$	-	Test cell volume
V_{water}	-	Volume of water
σ	-	Stefan-Boltzmann constant
ε_{water}	-	Emissivity of water
ε_{sky}	-	Emissivity of sky
ρ_{air}	-	Density of air
ρ_{water}	-	Density of water

APPENDIX II: BUILDING PROPERTIES

Table A2.1. Properties of building materials

Symbol:	Value	Units:	Description/ Notes
A_{roof}	3.964	m^2	Area of roof = 8' X 5' - 4" = 42.67 ft^2
A_{Floor}	2.698	m^2	Building floor area = 6'-10" x 4'-3" = 29.0417 ft^2
$A_{ceiling}$	2.698	m^2	Ceiling area = 6'-10" x 4'-3" = 29.0417 ft^2
$A_{Water\ surface}$	2.698	m^2	Area of water surface, same as the ceiling area
A_{w_North}	5.946	m^2	Area of north wall = 8' X 8' = 64 ft^2
A_{w_South}	5.946	m^2	Area of south wall = 8' X 8' = 64 ft^2
A_{w_East}	3.964	m^2	Area of east wall = 8' X 5' - 4" = 42.67 ft^2
A_{w_West}	3.964	m^2	Area of west wall = 8' X 5' - 4" = 42.67 ft^2
A_{Door}	1.905	m^2	Area of door (on east wall) = 3' X 6' -10" = 20.5 ft^2
$V_{test\text{-}cell}$	6.579	m^3	Test cell volume = 29.0417 ft^2 x 8 ft = 232.33 ft^3
L_W	0.229	m	Thickness of mass water = 9"
$h_{Air\_out\ (24\ Km/h)}$	34.000	$W / m^2 . °C$	h_o value ASHRAE fundamentals (24.2) [SI, 1997]
$h_{Air\_out\ (12\ Km/h)}$	22.000	$W / m^2 . °C$	h_o value ASHRAE fundamentals (24.2) [SI, 1997]
h_{conv_sky}		$W / m^2 . K$	$1.52 * (\Delta T)^{1/3}$
h_{rad_sky}		$W / m^2 . °C$	$[4 * \sigma * T'^3] / [1/\varepsilon_{water} + 1/\varepsilon_{sky} - 1]$ & $T' = (T_1 + T_2) / 2$
σ	0.00000006	-	$5.67 * 10^{-8}$
ε_{water}	0.930	$W / m^2 . K^4$	Emissivity of water
ε_{sky}	1.000	$W / m^2 . K^4$	Emissivity of sky
h_{Roof_panel}	0.516	$W / m^2 . °C$	Résistance of Roof panel is R = 11.0 (ft^2 . F°. h / Btu)
$h_{Air\ in\ 6"}$ (UP)	6.667	$W / m^2 . °C$	R = 0.15 [ASHRAE fundamentals SI, 1997 (24.2)]
$h_{Air\ in\ 6"}$ (DN)	5.263	$W / m^2 . °C$	R = 0.19 [ASHRAE fundamentals SI, 1997 (24.2)]
h_{water_1}	5.302	$W / m^2 . °C$	
h_{water_2}	5.302	$W / m^2 . °C$	
$CAPC_{water}$	712.758	$W / m^2 . °C$	

ρ	995.650	Kg /m^3 (21 °C)	CONVERT: $C_p = C_p$ x 1000 (J/KJ)
C_p	4178.400	J / Kg . K	Divide C_p by 3,600 sec to convert J.s into W.h
$h_{Air\ in\ still\ (UP)}$	9.260	W / m^2 . °C	h_i [ASHRAE fundamentals SI, 1997 (24.2)]
$h_{Air\ in\ still\ (DN)}$	6.130	W / m^2 . °C	h_i [ASHRAE fundamentals SI, 1997 (24.2)]
h_{Wall_North}	0.301	W / m^2 . °C	
h_{Wall_South}	0.301	W / m^2 . °C	
h_{Wall_East}	0.547	W / m^2 . °C	
h_{Wall_West}	0.301	W / m^2 . °C	
h_{Floor}	0.222	W / m^2 . °C	
UA_{Air_infil}	1.102	W / °C	Infiltration losses [UA_{Air_infil} = m . ρ . Cp]
m_{air}	0.001	m^3 / s	Mass flow rate of air [m = ACH . $V_{test\text{-}cell}$ / 3600 (seconds/hr)]
ρ	1.20	Kg /m^3	Density of air
C_p	1005.000	J / (Kg °C)	Specific heat of air
ACH	0.50	1 / h	Air changes per hour (Blower Door Test)

APPENDIX III: CALCULATION OF TEST CELL U-VALUES

Table A3.1. Construction properties of south wall

Building Element:	**R (at frame)**	**R (between frame)**
	(h ft^2 F° / Btu)	(h ft^2 F° / Btu)
Inside air resistance (vertical - flow horizontal)	0.68	0.68
Plywood siding (1/2")	0.62	0.62
Aluminum Foil (ignored)	-	-
2" x 6" (nominal) wood stud	5.50	-
1 3/4" air space with Aluminum foil (ε=0.03) on one side	3.99	3.99
Ridged Insulation (2")	-	9.80
Aluminum Foil (ignored)	-	-
1 3/4" air space with Aluminum foil (ε=0.03) on one side	3.99	3.99
Plywood siding (1/2")	0.62	0.62
Outside air resistance (7.5) mph	0.25	0.25
Sum	**15.65**	**19.95**

	Value	**Unit**
Area at frame	13.67	ft^2
Area between frame	41.00	ft^2
R - value (at frame)	15.65	(h ft^2 °F / Btu)
R - value (between frame)	19.95	(h ft^2 °F / Btu)
R - value (total)	18.87	(h ft^2 °F / Btu)
U - value	0.05	(Btu / h ft^2 °F)
h - value (per area)	**0.30**	**(W / m^2 °C)**

Table A3.2. Construction properties of north wall

Building Element:	**R (at frame)**	**R (between frame)**
	(h ft^2 F° / Btu)	(h ft^2 F° / Btu)
Inside air resistance (vertical - flow horizontal)	0.68	0.68
Plywood siding (1/2")	0.62	0.62
Aluminum Foil (ignored)	-	-
2" x 6" (nominal) wood stud	5.50	
1 3/4" air space with Aluminum foil (ε=0.03) on one side	3.99	3.99
Ridged Insulation (2")	-	9.80
Aluminum Foil (ignored)	-	-
1 3/4" air space with Aluminum foil (ε=0.03) on one side	3.99	3.99
Plywood siding (1/2")	0.62	0.62
Outside air resistance (7.5) mph	0.25	0.25
Sum	**15.65**	**19.95**

	Value	**Unit**
Area at frame	13.67	ft^2
Area between frame	41.00	ft^2
R - value (at frame)	15.65	(h ft^2 °F / Btu)
R - value (between frame)	19.95	(h ft^2 °F / Btu)
R - value (total)	18.87	(h ft^2 °F / Btu)
U - value	0.05	(Btu / h ft^2 °F)
h - value (per area)	**0.30**	**(W / m^2 °C)**

Table A3.3. Construction properties of west wall

Building Element:	**R (at frame)**	**R (between frame)**
	(h ft^2 F° / Btu)	(h ft^2 F° / Btu)
Inside air resistance (vertical - flow horizontal)	0.68	0.68
Plywood siding (1/2")	0.62	0.62
Aluminum Foil (ignored)	-	-
2" x 6" (nominal) wood stud	5.50	
1 3/4" air space with Aluminum foil (ε=0.03) on one side	3.99	3.99
Ridged Insulation (2")	-	9.80
Aluminum Foil (ignored)	-	-
1 3/4" air space with Aluminum foil (ε=0.03) on one side	3.99	3.99
Plywood siding (1/2")	0.62	0.62
Outside air resistance (7.5) mph	0.25	0.25
Sum	**15.65**	**19.95**

	Value	**Unit**
Area at frame	13.67	ft^2
Area between frame	41.00	ft^2
R - value (at frame)	15.65	(h ft^2 °F / Btu)
R - value (between frame)	19.95	(h ft^2 °F / Btu)
R - value (total)	18.87	(h ft^2 °F / Btu)
U - value	0.05	(Btu / h ft^2 °F)
h - value (per area)	**0.30**	**(W / m^2 °C)**

Table A3.4. Construction properties of east wall

Building Element:	**R (at frame)**	**R (between frame)**
Only wall	(h ft^2 F° / Btu)	(h ft^2 F° / Btu)
Inside air resistance (vertical - flow horizontal)	0.68	0.68
Plywood siding (1/2")	0.62	0.62
2" x 6" (nominal) wood stud	5.50	-
Tuff - R insulation 1.5"	-	7.50
5.5" insulation	-	19.00
Plywood siding (1/2")	0.62	0.62
Outside air resistance (7.5) mph	0.25	0.25
Sum	**7.67**	**28.67**

	Value	**Unit**
Area at frame	6.40	ft^2
Area between frame	12.80	ft^2
R - value (at frame)	7.67	(h ft^2 °F / Btu)
R - value (between frame)	28.67	(h ft^2 °F / Btu)
R - value of the wall (total)	21.67	(h ft^2 °F / Btu)
Door area	20.80	ft^2
R - value of the door	3.45	(h ft^2 °F / Btu)
R - value (total)	10.39	(h ft^2 °F / Btu)
U – value	0.10	(Btu / h ft^2 °F)
h - value (per area)	**0.55**	**(W / m^2 °C)**

Table A3.5. Construction properties of floor

Building Element:	**R (at frame)**	**R (between frame)**
	(h ft^2 F° / Btu)	**(h ft^2 F° / Btu)**
Inside air resistance (vertical - flow horizontal)	0.62	0.62
Plywood siding (1/2")	0.62	0.62
2" x 6" (nominal) wood stud	5.50	
Tuff - R insulation 1.5"		7.50
8" insulation		22.00
Plywood siding (1/2")	0.62	0.62
Outside air resistance (7.5) mph	0.25	0.25
Sum	**7.61**	**31.61**

	Value	**Unit**
Area at frame	7.25	ft^2
Area between frame	21.75	ft^2
R - value (at frame)	7.61	(h ft^2 °F / Btu)
R - value (between frame)	31.61	(h ft^2 °F / Btu)
R - value (total)	25.61	(h ft^2 °F / Btu)
U - value	0.04	(Btu / h ft^2 °F)
h - value (per area)	**0.22**	**(W / m^2 °C)**

Table A3.6. Construction properties of water mass

Upper half water mass

	Value	Unit
depth of water (L)	0.11	M
conductivity of water (k)	0.61	(W / m °C)
h_{water_1}	**5.302**	(W / m^2 °C)

Bottom half water mass

	Value	Unit
depth of water (L)	0.11	M
conductivity of water (k)	0.61	(W / m °C)
h_{water_2}	**5.302**	(W / m^2 °C)

Table A3.7. Construction properties of Martin™ Grage door, as insulation panel

	Value	Unit
R – value	11.00	(h ft^2 °F / Btu)
U – value	0.09	(Btu / h ft^2 °F)
h - value (per area)	**0.516**	(W / m^2 °C)

APPENDIX IV: CALCULATION OF U-VALUES FOR EACH NODE

1. Convection heat transfer coefficient of outside air (h_{Air_out}):

IF Wind Velocity >12 kph, h_{Air_out} = 22.0 W / m^2 °C, **or** h_{Air_out} = 34.0 W / m^2 °C)

Where, Wind Velocity is in kph, h_{Air_out} is in (W / m^2 °C)

Table A4.1. Outside air convection heat transfer coefficient:

Date	Time	Wind Velocity (kph)	h_{Air_out} (W / m^2 °C)
17-May	12:00 PM	4.5	22.0
17-May	1:00 AM	3.6	22.0
17-May	2:00 AM	4.3	22.0
17-May	3:00 AM	4.1	22.0
17-May	4:00 AM	2.9	22.0
17-May	5:00 AM	4.1	22.0
17-May	6:00 AM	5.4	22.0
17-May	7:00 AM	3.7	22.0
17-May	8:00 AM	5.6	22.0
17-May	9:00 AM	9.4	22.0
17-May	10:00 AM	12.3	34.0
17-May	11:00 AM	10.6	22.0
17-May	12:00 PM	10.0	22.0
17-May	1:00 PM	8.6	22.0
17-May	2:00 PM	9.8	22.0
17-May	3:00 PM	5.6	22.0
17-May	4:00 PM	8.4	22.0
17-May	5:00 PM	5.9	22.0
17-May	6:00 PM	8.7	22.0
17-May	7:00 PM	7.5	22.0
17-May	8:00 PM	2.6	22.0
17-May	9:00 PM	3.7	22.0
17-May	10:00 PM	5.9	22.0
17-May	11:00 PM	3.4	22.0

2. Convection heat loss/gain to the sky (h_{Conv_sky}):

$$h_{\mathrm{Conv\_sky}} = 1.52 \times (T_{\mathrm{a}} - T_{\mathrm{Roof_{air}}})^{1/3}$$

Table A4.2. Convection coefficient for the sky:

Date	Time	T_a	T_{Roof_air}	h_{conv_sky}
		(° C)	(°C)	(W / m^2 °C)
17-May	12:00 PM	27.5	30.0	2.1
17-May	1:00 AM	26.3	29.9	2.3
17-May	2:00 AM	25.2	28.5	2.2
17-May	3:00 AM	24.6	28.4	2.4
17-May	4:00 AM	24.4	27.9	2.3
17-May	5:00 AM	23.3	27.6	2.5
17-May	6:00 AM	23.9	27.3	2.3
17-May	7:00 AM	26.3	27.1	1.5
17-May	8:00 AM	28.9	26.9	1.9
17-May	9:00 AM	31.4	27.5	2.4
17-May	10:00 AM	34.2	28.1	2.8
17-May	11:00 AM	35.5	29.0	2.8
17-May	12:00 PM	36.2	30.0	2.8
17-May	1:00 AM	37.7	31.0	2.9
17-May	2:00 AM	38.2	31.5	2.9
17-May	3:00 AM	38.5	31.9	2.9
17-May	4:00 AM	37.2	32.4	2.6
17-May	5:00 AM	35.9	32.7	2.3
17-May	6:00 AM	35.7	32.6	2.2
17-May	7:00 AM	35.0	32.0	2.2
17-May	8:00 AM	34.8	31.7	2.2
17-May	9:00 AM	31.9	31.7	0.9
17-May	10:00 AM	30.8	31.5	1.3
17-May	11:00 AM	29.7	30.7	1.5

3. Radiative heat loss/gain to the sky (h_{Rad_sky}):

$$h_{\text{Rad\_sky}} = \frac{4 \times \sigma \times T'^3}{\frac{1}{\varepsilon_{water}} + \frac{1}{\varepsilon_{sky}} - 1}$$

Where,

$\sigma = 5.67 * 10^{-8}$ W / m^2 . K^4 is Stefan-Boltzmann constant; T' = [(T_a + T_{sky}) / 2] in Kelvin scale; ε_{water} = 0.93, emissivity of water; ε_{sky} = 1.00, emissivity of sky.

Table A4.3. Radiative coefficient for the sky:

Date	Time	T_a	T_{sky}	h_{rad_sky}
		(° C)	(° C)	(W / m^2 °C)
17-May	12:00 PM	27.5	14.5	5.4
17-May	1:00 AM	26.3	12.8	5.3
17-May	2:00 AM	25.2	11.3	5.2
17-May	3:00 AM	24.6	10.3	5.2
17-May	4:00 AM	24.4	10.1	5.2
17-May	5:00 AM	23.3	8.5	5.1
17-May	6:00 AM	23.9	9.3	5.1
17-May	7:00 AM	26.3	12.8	5.3
17-May	8:00 AM	28.9	16.6	5.5
17-May	9:00 AM	31.4	20.2	5.6
17-May	10:00 AM	34.2	24.2	5.8
17-May	11:00 AM	35.5	26.1	5.9
17-May	12:00 PM	36.2	27.2	6.0
17-May	1:00 AM	37.7	29.3	6.1
17-May	2:00 AM	38.2	30.0	6.1
17-May	3:00 AM	38.5	30.5	6.1
17-May	4:00 AM	37.2	28.6	6.0
17-May	5:00 AM	35.9	26.7	5.9
17-May	6:00 AM	35.7	26.3	5.9
17-May	7:00 AM	35.0	25.3	5.9
17-May	8:00 AM	34.8	25.0	5.9
17-May	9:00 AM	31.9	20.9	5.7
17-May	10:00 AM	30.8	19.3	5.6
17-May	11:00 AM	29.7	17.6	5.5

4. Convection heat transfer coefficient between the night sky and the water mass ($h_{Outside\_NO\ Panel}$):

$$h_{\text{Outside\_NO Panel}} = \frac{1}{\frac{1}{h_{Air\_out}} + \frac{1}{h_{Conv\_sky}} + \frac{1}{h_{Rad\_Sky}}}$$

Table A4.4. Convection coefficient for the night sky and the water mass:

Date	Time	h_{Air_out}	h_{conv_sky}	h_{rad_sky}	$h_{Outside\_NO\ Panel}$
		(W / m^2 °C)	(W / m^2 °C)	(W / m^2 °C)	(W / m^2 °C)
17-May	12:00 PM	22.0	2.1	5.4	1.4
17-May	1:00 AM	22.0	2.3	5.3	1.5
17-May	2:00 AM	22.0	2.2	5.2	1.5
17-May	3:00 AM	22.0	2.4	5.2	1.5
17-May	4:00 AM	22.0	2.3	5.2	1.5
17-May	5:00 AM	22.0	2.5	5.1	1.5
17-May	6:00 AM	22.0	2.3	5.1	1.5
17-May	7:00 AM	22.0	1.5	5.3	1.1
17-May	8:00 AM	22.0	1.9	5.5	1.3
17-May	9:00 AM	22.0	2.4	5.6	1.6
17-May	10:00 AM	34.0	2.8	5.8	1.8
17-May	11:00 AM	22.0	2.8	5.9	1.8
17-May	12:00 PM	22.0	2.8	6.0	1.8
17-May	1:00 AM	22.0	2.9	6.1	1.8
17-May	2:00 AM	22.0	2.9	6.1	1.8
17-May	3:00 AM	22.0	2.9	6.1	1.8
17-May	4:00 AM	22.0	2.6	6.0	1.7
17-May	5:00 AM	22.0	2.3	5.9	1.5
17-May	6:00 AM	22.0	2.2	5.9	1.5
17-May	7:00 AM	22.0	2.2	5.9	1.5
17-May	8:00 AM	22.0	2.2	5.9	1.5
17-May	9:00 AM	22.0	0.9	5.7	0.8
17-May	10:00 AM	22.0	1.3	5.6	1.0
17-May	11:00 AM	22.0	1.5	5.5	1.1

5. Convection heat transfer coefficient between the sky and the roof panel ($h_{Outside\_Panel}$):

$$h_{\text{Outside\_Panel}} = \frac{1}{\frac{1}{h_{Air\_out} + h_{Conv\_sky} + h_{Rad\_sky}} + \frac{1}{h_{Roof\_panel}}}$$

Table A4.5. Convection coefficient for the night sky and the roof panel:

Date	Time	h_{Air_out}	h_{conv_sky}	h_{rad_sky}	h_{Roof_panel}	$h_{Outside\_Panel}$
		(W / m^2 °C)	(W / m^2 °C)	(W / m^2 °C)	(W / m^2 °C)	(W / m^2 °C)
17-May	12:00 PM	22.0	2.1	5.4	0.5	0.5
17-May	1:00 AM	22.0	2.3	5.3	0.5	0.5
17-May	2:00 AM	22.0	2.2	5.2	0.5	0.5
17-May	3:00 AM	22.0	2.4	5.2	0.5	0.5
17-May	4:00 AM	22.0	2.3	5.2	0.5	0.5
17-May	5:00 AM	22.0	2.5	5.1	0.5	0.5
17-May	6:00 AM	22.0	2.3	5.1	0.5	0.5
17-May	7:00 AM	22.0	1.5	5.3	0.5	0.5
17-May	8:00 AM	22.0	1.9	5.5	0.5	0.5
17-May	9:00 AM	22.0	2.4	5.6	0.5	0.5
17-May	10:00 AM	34.0	2.8	5.8	0.5	0.5
17-May	11:00 AM	22.0	2.8	5.9	0.5	0.5
17-May	12:00 PM	22.0	2.8	6.0	0.5	0.5
17-May	1:00 AM	22.0	2.9	6.1	0.5	0.5
17-May	2:00 AM	22.0	2.9	6.1	0.5	0.5
17-May	3:00 AM	22.0	2.9	6.1	0.5	0.5
17-May	4:00 AM	22.0	2.6	6.0	0.5	0.5
17-May	5:00 AM	22.0	2.3	5.9	0.5	0.5
17-May	6:00 AM	22.0	2.2	5.9	0.5	0.5
17-May	7:00 AM	22.0	2.2	5.9	0.5	0.5
17-May	8:00 AM	22.0	2.2	5.9	0.5	0.5
17-May	9:00 AM	22.0	0.9	5.7	0.5	0.5
17-May	10:00 AM	22.0	1.3	5.6	0.5	0.5
17-May	11:00 AM	22.0	1.5	5.5	0.5	0.5

6. Convective heat transfer coefficient for the 6" (15.24 cm) air-gap ($h_{Air\_in\_6"}$):

IF $T_{Roof\_air} > T_a$, $h_{Air\_in\_6"}$ is upwards, **or** $h_{Air\_in\_6"}$ is downwards

$h_{\mathrm{Air\_in\_6"}}\,(UP) = 6.7$ W / m^2. °C (ASHRAE, 2009)

$h_{\mathrm{Air\_in\_6"}}\,(DN) = 5.3$ W / m^2. °C (ASHRAE, 2009)

Table A4.6. Convection coefficient for the air-gap:

Date	Time	T_{Roof_air} (°C)	T_a (°C)	$h_{Air\_in\_6"}$ (W / m^2 °C)
17-May	12:00 PM	30.0	28.0	6.7
17-May	1:00 AM	29.9	27.5	6.7
17-May	2:00 AM	28.5	26.3	6.7
17-May	3:00 AM	28.4	25.2	6.7
17-May	4:00 AM	27.9	24.6	6.7
17-May	5:00 AM	27.6	24.4	6.7
17-May	6:00 AM	27.3	23.3	6.7
17-May	7:00 AM	27.1	23.9	6.7
17-May	8:00 AM	26.9	26.3	6.7
17-May	9:00 AM	27.5	28.9	5.3
17-May	10:00 AM	28.1	31.4	5.3
17-May	11:00 AM	29.0	34.2	5.3
17-May	12:00 PM	30.0	35.5	5.3
17-May	1:00 AM	31.0	36.2	5.3
17-May	2:00 AM	31.5	37.7	5.3
17-May	3:00 AM	31.9	38.2	5.3
17-May	4:00 AM	32.4	38.5	5.3
17-May	5:00 AM	32.7	37.2	5.3
17-May	6:00 AM	32.6	35.9	5.3
17-May	7:00 AM	32.0	35.7	5.3
17-May	8:00 AM	31.7	35.0	5.3
17-May	9:00 AM	31.7	34.8	5.3
17-May	10:00 AM	31.5	31.9	5.3
17-May	11:00 AM	30.7	30.8	5.3

7. Convective heat transfer coefficient for still air under the ceiling ($h_{Air\_in\_still}$):

IF $T_{Roof\_air} > T_a$, $h_{Air\_in\_still}$ is upwards, **or** $h_{Air\_in\_still}$ is downwards

$h_{\mathrm{Air\_in\_still}}\ (UP) = 9.3$ W / m^2. °C (ASHRAE, 2009)

$h_{\mathrm{Air\_in\_still}}\ (DN) = 6.1$ W / m^2. °C (ASHRAE, 2009)

Table A4.7. Convection coefficient for the indoor still air:

Date	Time	T_{in_calc} (°C)	$T_{Ceiling}$ (°C)	$h_{Air\_in\_still}$ (W / m^2 °C)
17-May	12:00 PM	25.0	28.0	6.1
17-May	1:00 AM	27.2	26.8	9.3
17-May	2:00 AM	27.7	27.9	6.1
17-May	3:00 AM	27.5	28.2	6.1
17-May	4:00 AM	27.1	28.1	6.1
17-May	5:00 AM	26.8	27.9	6.1
17-May	6:00 AM	26.4	27.7	6.1
17-May	7:00 AM	26.3	27.5	6.1
17-May	8:00 AM	27.3	27.4	6.1
17-May	9:00 AM	29.2	27.9	9.3
17-May	10:00 AM	30.9	29.0	9.3
17-May	11:00 AM	32.0	30.1	9.3
17-May	12:00 PM	32.5	30.8	9.3
17-May	1:00 AM	33.1	31.1	9.3
17-May	2:00 AM	34.0	31.5	9.3
17-May	3:00 AM	35.6	32.2	9.3
17-May	4:00 AM	36.8	33.3	9.3
17-May	5:00 AM	36.2	34.1	9.3
17-May	6:00 AM	34.9	33.7	9.3
17-May	7:00 AM	33.9	32.9	9.3
17-May	8:00 AM	33.1	32.3	9.3
17-May	9:00 AM	32.6	31.9	9.3
17-May	10:00 AM	32.0	31.6	9.3
17-May	11:00 AM	31.3	31.2	9.3

APPENDIX V: CALCULATION OF TEMPERATUERE AT EACH NODE

1. Node-1: Top of the roof surface (T_{Roof_air}):

$$T_{\text{Roof\_air}} = \frac{(UA_{Outside\_panel} \times T_a) + (UA_{Air\_6"\_in} \times T_{Water\_surf})}{UA_a + UA_{Water\_surf}}$$

Table A5.1. Temperature of the roof surface:

Date	Time	$UA_{Outside\_Panel}$ (W / °C)	$UA_{Air\_6"\_in}$ (W / °C)	T_a (°C)	T_{Water_surf} (°C)	T_{Roof_air} (°C)
17-May	12:00 PM	2.0	18.0	27.5	28.6	29.8
17-May	1:00 AM	2.0	18.0	26.3	28.5	28.3
17-May	2:00 AM	2.0	18.0	25.2	28.2	28.2
17-May	3:00 AM	2.0	18.0	24.6	27.8	27.8
17-May	4:00 AM	2.0	18.0	24.4	27.6	27.5
17-May	5:00 AM	2.0	18.0	23.3	27.5	27.2
17-May	6:00 AM	2.0	18.0	23.9	27.2	27.1
17-May	7:00 AM	2.0	18.0	26.3	27.6	27.1
17-May	8:00 AM	2.0	18.0	28.9	28.0	26.3
17-May	9:00 AM	2.0	14.2	31.4	28.7	28.1
17-May	10:00 AM	2.0	14.2	34.2	29.5	28.2
17-May	11:00 AM	2.0	14.2	35.5	30.5	29.1
17-May	12:00 PM	2.0	14.2	36.2	30.9	29.1
17-May	1:00 AM	2.0	14.2	37.7	31.3	29.8
17-May	2:00 AM	2.0	14.2	38.2	31.8	29.9
17-May	3:00 AM	2.0	14.2	38.5	32.0	30.2
17-May	4:00 AM	2.0	14.2	37.2	32.1	30.2
17-May	5:00 AM	2.0	14.2	35.9	31.6	30.2
17-May	6:00 AM	2.0	14.2	35.7	31.3	30.3
17-May	7:00 AM	2.0	14.2	35.0	31.3	30.3
17-May	8:00 AM	2.0	14.2	34.8	31.2	30.3
17-May	9:00 AM	2.0	14.2	31.9	30.6	29.8
17-May	10:00 AM	2.0	14.2	30.8	30.2	30.7
17-May	11:00 AM	2.0	14.2	29.7	30.1	29.9

Node-2: Top surface of the water mass (T_{Water_surf}):

$$T_{\text{Water\_surf}} = \frac{(UA_{Effective} \times T_{Effective}) + (UA_{Water\_1} \times T_{Water})}{UA_{Effective} + UA_{Water}}$$

From 6:00 AM – 6:59 PM, $UA_{Effective} = UA_{Air\_6"\_in}$ **and** $T_{Effective} = T_{Roof\_air}$

From 7:00 PM – 5:59 AM, $UA_{Effective} = UA_{Outside\_No\ Panel}$ **and** $T_{Effective} = T_a$

Table A5.2. Top surface temperature of the water mass:

Date	Time	$UA_{Effective}$	UA_{water_1}	$T_{Effective}$	T_{Water}	T_{Water_surf}
		(W / °C)	(W / °C)	(°C)	(°C)	(°C)
17-May	12:00 PM	5.5	14.3	27.5	29.0	28.6
17-May	1:00 AM	6.0	14.3	26.3	28.9	28.5
17-May	2:00 AM	5.8	14.3	25.2	28.9	28.2
17-May	3:00 AM	6.0	14.3	24.6	28.8	27.8
17-May	4:00 AM	5.9	14.3	24.4	28.8	27.6
17-May	5:00 AM	6.1	14.3	23.3	28.8	27.5
17-May	6:00 AM	5.9	14.3	23.9	28.7	27.2
17-May	7:00 AM	4.3	14.3	27.1	28.7	27.6
17-May	8:00 AM	5.3	14.3	26.3	28.6	28.0
17-May	9:00 AM	6.2	14.3	28.1	28.6	28.7
17-May	10:00 AM	7.1	14.3	28.2	28.6	29.5
17-May	11:00 AM	7.0	14.3	29.1	28.7	30.5
17-May	12:00 PM	6.9	14.3	29.1	28.8	30.9
17-May	1:00 AM	7.1	14.3	29.8	28.9	31.3
17-May	2:00 AM	7.1	14.3	29.9	29.0	31.8
17-May	3:00 AM	7.1	14.3	30.2	29.1	32.0
17-May	4:00 AM	6.6	14.3	30.2	29.3	32.1
17-May	5:00 AM	6.0	14.3	30.2	29.4	31.6
17-May	6:00 AM	6.0	14.3	30.3	29.5	31.3
17-May	7:00 AM	5.9	14.3	30.3	29.6	31.3
17-May	8:00 AM	5.9	14.3	34.8	29.7	31.2
17-May	9:00 AM	3.0	14.3	31.9	29.8	30.6
17-May	10:00 AM	4.0	14.3	30.8	29.8	30.2
17-May	11:00 AM	4.5	14.3	29.7	29.9	30.1

Node-3: Bottom of the water mass (T_{Water}):

$$T_{\text{Water }(n=1)} = \left[T_{Water\ (n=0)}\right] + \left[\frac{\left\{UA_{Water_1} \times \left(T_{Water_{surf}} - T_{\text{Roof}_{\text{air}(n=0)}}\right)\right\} + \left\{UA_{Water_2} \times \left(T_{Ceiling} - T_{\text{Roof}_{\text{air}(n=0)}}\right)\right\}}{CAPC}\right]$$

Table A5.3. Bottom surface temperature of the water mass:

Date	Time	UA_{water_1}	UA_{water_2}	CAPC	T_{Water_surf}	$T_{Ceiling}$	T_{Water}
		(W / °C)	(W / °C)	(Wh / °C)	(°C)	(°C)	(°C)
17-May	12:00 PM	14.3	14.3	712.8	28.6	28.0	29.0
17-May	1:00 AM	14.3	14.3	712.8	28.5	26.8	28.9
17-May	2:00 AM	14.3	14.3	712.8	28.2	27.9	28.9
17-May	3:00 AM	14.3	14.3	712.8	27.8	28.2	28.8
17-May	4:00 AM	14.3	14.3	712.8	27.6	28.1	28.8
17-May	5:00 AM	14.3	14.3	712.8	27.5	27.9	28.8
17-May	6:00 AM	14.3	14.3	712.8	27.2	27.7	28.7
17-May	7:00 AM	14.3	14.3	712.8	27.6	27.5	28.7
17-May	8:00 AM	14.3	14.3	712.8	28.0	27.4	28.6
17-May	9:00 AM	14.3	14.3	712.8	28.7	27.9	28.6
17-May	10:00 AM	14.3	14.3	712.8	29.5	29.0	28.6
17-May	11:00 AM	14.3	14.3	712.8	30.5	30.1	28.7
17-May	12:00 PM	14.3	14.3	712.8	30.9	30.8	28.8
17-May	1:00 AM	14.3	14.3	712.8	31.3	31.1	28.9
17-May	2:00 AM	14.3	14.3	712.8	31.8	31.5	29.0
17-May	3:00 AM	14.3	14.3	712.8	32.0	32.2	29.1
17-May	4:00 AM	14.3	14.3	712.8	32.1	33.3	29.3
17-May	5:00 AM	14.3	14.3	712.8	31.6	34.1	29.4
17-May	6:00 AM	14.3	14.3	712.8	31.3	33.7	29.5
17-May	7:00 AM	14.3	14.3	712.8	31.3	32.9	29.6
17-May	8:00 AM	14.3	14.3	712.8	31.2	32.3	29.7
17-May	9:00 AM	14.3	14.3	712.8	30.6	31.9	29.8
17-May	10:00 AM	14.3	14.3	712.8	30.2	31.6	29.8
17-May	11:00 AM	14.3	14.3	712.8	30.1	31.2	29.9

Node-4: Bottom of the ceiling ($T_{Ceiling}$):

$$T_{\text{Ceiling}} = \frac{(UA_{Water\_2} \times T_{Water}) + (UA_{Air\_in\_still} \times T_{In})}{UA_{Water\_2} + UA_{Air\_in\_still}}$$

Table A5.4. Bottom surface temperature of the ceiling:

Date	Time	UA_{water_2}	$UA_{Air\_in\_still}$	T_{Water}	T_{in_calc}	$T_{Ceiling}$
		(W / °C)	(W / °C)	(°C)	(°C)	(°C)
17-May	12:00 PM	14.3	16.5	29.0	25.0	26.8
17-May	1:00 AM	14.3	25.0	28.9	27.2	27.9
17-May	2:00 AM	14.3	16.5	28.9	27.7	28.2
17-May	3:00 AM	14.3	16.5	28.8	27.5	28.1
17-May	4:00 AM	14.3	16.5	28.8	27.1	27.9
17-May	5:00 AM	14.3	16.5	28.8	26.8	27.7
17-May	6:00 AM	14.3	16.5	28.7	26.4	27.5
17-May	7:00 AM	14.3	16.5	28.7	26.3	27.4
17-May	8:00 AM	14.3	16.5	28.6	27.3	27.9
17-May	9:00 AM	14.3	25.0	28.6	29.2	29.0
17-May	10:00 AM	14.3	25.0	28.6	30.9	30.1
17-May	11:00 AM	14.3	25.0	28.7	32.0	30.8
17-May	12:00 PM	14.3	25.0	28.8	32.5	31.1
17-May	1:00 AM	14.3	25.0	28.9	33.1	31.5
17-May	2:00 AM	14.3	25.0	29.0	34.0	32.2
17-May	3:00 AM	14.3	25.0	29.1	35.6	33.3
17-May	4:00 AM	14.3	25.0	29.3	36.8	34.1
17-May	5:00 AM	14.3	25.0	29.4	36.2	33.7
17-May	6:00 AM	14.3	25.0	29.5	34.9	32.9
17-May	7:00 AM	14.3	25.0	29.6	33.9	32.3
17-May	8:00 AM	14.3	25.0	29.7	33.1	31.9
17-May	9:00 AM	14.3	25.0	29.8	32.6	31.6
17-May	10:00 AM	14.3	25.0	29.8	32.0	31.2
17-May	11:00 AM	14.3	25.0	29.9	31.3	30.8

Node-5: Indoor air temperature (T_{in_calc}):

$$T_{\text{in\_calc}} = \frac{\begin{array}{c}\left(UA_{Air\_in\_still} \times T_{Ceiling}\right) + \left(UA_{Air\_infill} \times T_a\right) + \\ \left(UA_{Wall\_north} \times T_{Wall\_north}\right) + \left(UA_{Wall\_south} \times T_{Wall\_south}\right) + \\ \left(UA_{Wall\_east} \times T_{Wall\_east}\right) + \left(UA_{Wall\_west} \times T_{Wall\_west}\right) + \left(UA_{Floor} \times T_{Floor}\right)\end{array}}{\begin{array}{c}[\, UA_{Air_{in_{still}}} + UA_{Air_{infill}} + UA_{Wall_{north}} + UA_{Wall_{south}} + \\ UA_{Wall\_east} + UA_{Wall\_west} + UA_{Floor}\,]\end{array}}$$

Table A5.5. UA values for the surfaces connected to node-5:

Date	Time	$UA_{Air\_in\_still}$ (W / °C)	UA_{Air_infil} (W / °C)	UA_{Wall_North} (W / °C)	UA_{Wall_South} (W / °C)	UA_{Wall_East} (W / °C)	UA_{Wall_West} (W / °C)	UA_{Floor} (W / °C)
17-May	12:00 PM	16.5	1.1	1.8	1.8	2.2	1.2	0.6
17-May	1:00 AM	25.0	1.1	1.8	1.8	2.2	1.2	0.6
17-May	2:00 AM	16.5	1.1	1.8	1.8	2.2	1.2	0.6
17-May	3:00 AM	16.5	1.1	1.8	1.8	2.2	1.2	0.6
17-May	4:00 AM	16.5	1.1	1.8	1.8	2.2	1.2	0.6
17-May	5:00 AM	16.5	1.1	1.8	1.8	2.2	1.2	0.6
17-May	6:00 AM	16.5	1.1	1.8	1.8	2.2	1.2	0.6
17-May	7:00 AM	16.5	1.1	1.8	1.8	2.2	1.2	0.6
17-May	8:00 AM	16.5	1.1	1.8	1.8	2.2	1.2	0.6
17-May	9:00 AM	25.0	1.1	1.8	1.8	2.2	1.2	0.6
17-May	10:00 AM	25.0	1.1	1.8	1.8	2.2	1.2	0.6
17-May	11:00 AM	25.0	1.1	1.8	1.8	2.2	1.2	0.6
17-May	12:00 PM	25.0	1.1	1.8	1.8	2.2	1.2	0.6
17-May	1:00 AM	25.0	1.1	1.8	1.8	2.2	1.2	0.6
17-May	2:00 AM	25.0	1.1	1.8	1.8	2.2	1.2	0.6
17-May	3:00 AM	25.0	1.1	1.8	1.8	2.2	1.2	0.6
17-May	4:00 AM	25.0	1.1	1.8	1.8	2.2	1.2	0.6
17-May	5:00 AM	25.0	1.1	1.8	1.8	2.2	1.2	0.6
17-May	6:00 AM	25.0	1.1	1.8	1.8	2.2	1.2	0.6
17-May	7:00 AM	25.0	1.1	1.8	1.8	2.2	1.2	0.6
17-May	8:00 AM	25.0	1.1	1.8	1.8	2.2	1.2	0.6

17-May	9:00 AM	25.0	1.1	1.8	1.8	2.2	1.2	0.6
17-May	10:00 AM	25.0	1.1	1.8	1.8	2.2	1.2	0.6
17-May	11:00 AM	25.0	1.1	1.8	1.8	2.2	1.2	0.6

Table A5.6. Calculated indoor air temperature:

Date	Time	$T_{Ceiling}$	T_a	T_{Wall_North}	T_{Wall_South}	T_{Wall_East}	T_{Wall_West}	T_{Floor}	T_{in_calc}
		(°C)	(°C)	(°C)	(°C)	(°C)	(°C)	(°C)	(°C)
17-May	12:00 PM	26.8	27.5	28.4	28.4	28.4	25.0	31.2	27.2
17-May	1:00 AM	27.9	26.3	27.5	27.5	27.5	24.4	30.1	27.7
17-May	2:00 AM	28.2	25.2	26.4	26.4	26.4	23.6	29.1	27.5
17-May	3:00 AM	28.1	24.6	25.5	25.5	25.5	23.1	28.1	27.1
17-May	4:00 AM	27.9	24.4	25.0	24.9	24.9	22.5	27.1	26.8
17-May	5:00 AM	27.7	23.3	24.1	24.1	24.1	21.6	26.0	26.4
17-May	6:00 AM	27.5	23.9	24.1	24.1	24.1	23.3	25.5	26.3
17-May	7:00 AM	27.4	26.3	28.6	26.3	26.3	28.9	25.2	27.3
17-May	8:00 AM	27.9	28.9	31.0	32.6	32.6	34.6	25.4	29.2
17-May	9:00 AM	29.0	31.4	33.3	40.6	40.6	37.5	26.0	30.9
17-May	10:00 AM	30.1	34.2	37.1	39.6	39.6	38.8	26.9	32.0
17-May	11:00 AM	30.8	35.5	38.6	37.8	37.8	40.5	28.3	32.5
17-May	12:00 PM	31.1	36.2	39.7	38.7	38.7	43.8	29.6	33.1
17-May	1:00 AM	31.5	37.7	40.9	41.0	41.0	49.4	30.9	34.0
17-May	2:00 AM	32.2	38.2	42.8	51.3	51.3	45.4	32.2	35.6
17-May	3:00 AM	33.3	38.5	43.5	53.4	53.4	45.4	33.6	36.8
17-May	4:00 AM	34.1	37.2	41.0	45.0	45.0	45.4	34.9	36.2
17-May	5:00 AM	33.7	35.9	38.1	38.4	38.4	40.3	36.0	34.9
17-May	6:00 AM	32.9	35.7	36.6	36.7	36.7	36.4	36.5	33.9
17-May	7:00 AM	32.3	35.0	35.7	35.7	35.7	34.4	36.6	33.1
17-May	8:00 AM	31.9	34.8	34.8	34.9	34.9	32.7	36.3	32.6
17-May	9:00 AM	31.6	31.9	33.6	33.6	33.6	30.7	35.6	32.0
17-May	10:00 AM	31.2	30.8	32.1	32.1	32.1	29.2	34.5	31.3
17-May	11:00 AM	30.8	29.7	31.3	31.3	31.3	28.6	33.4	30.8

APPENDIX VI: PREDICTED TEMPERATURE

Table A6.1. Predicted indoor temperature using different models:

Date	Time	$T_{in\_measured}$	T_{in_calc}	T_{time_series}	AR (1)	AR (2)	ARIMA (1,0,1)
		(°C)	(°C)	(°C)	(°C)	(°C)	(°C)
17-May	12:00 PM	30.2	27.2	27.1	27.1	27.1	27.1
17-May	1:00 AM	29.0	27.7	26.9	26.2	26.9	26.6
17-May	2:00 AM	27.9	27.5	26.7	25.8	25.8	26.2
17-May	3:00 AM	27.0	27.1	26.2	25.4	25.5	25.7
17-May	4:00 AM	26.0	26.8	25.7	25.1	25.3	25.3
17-May	5:00 AM	25.1	26.4	25.1	24.7	24.8	24.8
17-May	6:00 AM	24.9	26.3	24.7	24.8	25.0	24.7
17-May	7:00 AM	25.2	27.3	24.6	24.7	24.7	24.7
17-May	8:00 AM	25.6	29.2	24.8	24.8	24.8	24.9
17-May	9:00 AM	27.1	30.9	25.0	24.6	24.5	24.7
17-May	10:00 AM	28.7	32.0	25.3	25.2	25.3	25.2
17-May	11:00 AM	30.4	32.5	25.7	25.5	25.5	25.6
17-May	12:00 PM	31.9	33.1	26.2	26.0	26.0	26.1
17-May	1:00 AM	33.4	34.0	26.6	26.2	26.2	26.4
17-May	2:00 AM	34.9	35.6	26.9	26.6	26.6	26.7
17-May	3:00 AM	36.2	36.8	26.9	26.6	26.7	26.7
17-May	4:00 AM	37.5	36.2	27.1	26.9	27.0	27.0
17-May	5:00 AM	37.9	34.9	27.2	27.2	27.3	27.3
17-May	6:00 AM	37.5	33.9	27.3	27.2	27.1	27.2
17-May	7:00 AM	37.1	33.1	27.3	27.1	27.1	27.2
17-May	8:00 AM	36.6	32.6	27.1	27.0	27.0	27.0
17-May	9:00 AM	35.1	32.0	27.0	26.9	26.9	27.0
17-May	10:00 AM	33.6	31.3	27.0	26.7	26.7	26.8
17-May	11:00 AM	32.6	30.8	26.8	26.5	26.5	26.7

REFERENCES

Ahmed, I. (1985). Improving the thermal performance of a roof pond system. *Energy Conversion Management*, *25* (2), 207-209.

ASHRAE. (2009). *ASHRAE Handbook: Fundamentals*. (IP Edition). Atlanta: American Society of Heating, Refrigerating and Air-Conditioning Engineers, Inc.

Balcomb, J. D. (1992). *Passive solar buildings*. Cambridge: The MIT Press.

Bliss, R. W. (1961). Atmospheric radiation near the surface of the earth. *Solar Energy, 5*, 103-120.

Carrasco, A., Pittard, R., Kondepudi, S., & Somasundaram, S. (1987). Evaluation of a direct evaporative roof-spray cooling system. *4th Annual Symposium on Imroving Building Energy Efficiency in Hot and Humid Climates.* Huston, TX: Texas A&M University.

Chandra, S., Kaushik, S. C., & Bansal, P. K. (1985). Thermal performance of a non-air-conditioned building for passive solar air-conditioning: Evaluation of roof cooling systems. *Energy and Buildings, 8* (1), 51-69.

Clarck, G., Loxsom, F., Allen, C., & Treat, C. H. (1985). *Assessment of passive cooling rates and applications in the United States*, Report prepared by Trinity University for U.S. D.O.E., Contract EG-77-C-05-1600.

Chen, B., Guenther, R., Kasher, J., & Maloney, J. (1988). Modeling of the radiative, convective, and evaporative heat transfer mechanism of the Nebraska modified roof pond for the determination of cooling performance curves. *Proceedings of the 13th National Passive Solar Conference*. 13, pp. 343-348. Boulder, CA: American Solar Energy Society.

Cook, J. (1985). *Passive cooling.* Cambridge, MA, USA: MIT Press.

Crowther, K., & Melzer, B. (1979). The thermosiphoning cool pool: a natural cooling system. *Proc III: National Passive Solar Conference.* CA: American Section of ISES.

EIA. (2010). *Annual Energy Review 2009.* Washington, DC: U.S. Department of Energy.

Fernández-González, A. (2007). Analysis of the thermal performance and comfort conditions produced by five different passive solar heating strategies in the United States midwest. *Solar Energy, 81*, 581-593.

Fernandez-Gonzalez, A., & Hossain, A. (2010). Cooling performance and energy savings produced by a roofpond in the united states southwest. *American Solar Energy Society National Solar Conference 2010*, Phoenix, AZ.

Givoni, B. (1999). Minimum climatic information needed to predict performance of passive buildings in hot climates. *Passive and Low Energy Architecture Conference 1999*, Brisbane, Australia.

Givoni, B. (1994). *Passive and low energy cooling of buildings.* NY: Van Nostrand Reinhold.

Haggard, K. L. (1977). The architecture of a passive system of diurnal radiation heating and cooling. *Solar Energy, 19*, 403-406.

Haggard, K. L., Edmiston, J. W., Feldman, J., Hawes, M., & Niles, P. W. (1975). *Research evaluation of a system of natural air conditioning: Final report [Roof ponds and movable insulation].* California Polytechnic State University, Department of Energy. Washington, D.C.: Department of Housing and Urban Development.

Hassid, S., & Geros, V. (2006). Heat and mass transfer phenomena in urban buildings. In M. Santamouris (Ed.), *Environmental design of urban buildings: An integrated approach* (p. 127). London: Earthscan.

Hay, H. R., & Yellott, J. (1968). International aspects of air conditioning with movable insulation. *Solar Energy*, *12*, 427-438.

Hoffstatter, L. S. (1985). Environmental heat transfer for roof pond heating. *Unpublished Masters' Thesis*. San Antonio, TX: Trinity University.

Hossain, A., & Fernandez-Gonzalez, A. (2012). Development and validation of a thermal network model to predict indoor operative temperatures in dry roofpond buildings. *World Renewable Energy Forum 2012*, Denver, CO.

Jain, D. (2006). Modeling of solar passive techniques for roof cooling in arid regions. *Building and Environment*, 41, 277-287.

Kako, I. K. (2009). Empirically derived formulas to predict indoor maximum, average, and minimum temperatures in roofpond buildings using minimum climatic information. *Unpublished Masters' Thesis*. Las Vegas, NV: University of Nevada, Las Vegas.

Kreider, J., Curtiss, P., & Rabl, A. (2010). *Heating and cooling of buildings*. (2nd ed.). New York: CRC Press.

Lord, D. (1999). *An interactive, web-based computer program for thermal design of roof ponds.* San Luis Obispo, CA: California Polytechnic State University.

Marlatt, W. P., Murray, K. A., & Squier, S. E. (1984). *Roof pond systems.* Energy Systems Group, Rockwell International., U.S. Department of Energy. Canoga Park, CA: Energy Technology Engineering Center.

Mazria, E. (1979). *The passive solar energy book.* Emmaus, PA: Rodale Press.

Nahar, N. M., Sharma, P., & Puurohit, N. M. (1999). Studies on solar passive cooling techniques for arid areas. *Energy Conversion and Management*, *45*, 89-95.

Schutt, B. L. (1984). Heat transfer to the nocturnal environment for roof pond cooling. *Unpublished Masters' Thesis*. San Antonio, TX: Trinity University.

Sodha, M. S., Govind, Bansal, P. K., & Kaushik, S. C. (1980). Reduction of heat flux by a flowing water layer over and insulated roof. *Building and Environment*, *15*, 133-140.

Sodha, M. S., Kumar, A., Tiwari, G. N., & Tyagi, R. C. (1981). Simple multiple wick solar still: analysis and performance. *Solar Energy*, *26*, 127-131.

Spanaki, A. (2007). Comparative studies on different type of roof ponds for cooling purposes. *2nd PALENC Conference and 28th AIVC Conference on Building Low Energy Cooling and Advanced Ventilation Technologies in the 21st Century* (pp. 1009-1015). Crete island, Greece: PalencAIVC.

Tiwari, G. N., Lugani, N., & Singh, A. K. (1993). Design parameters of a non-air-conditioned cinema hall for thermal comfort under arid-zone climate conditions. *Energy Buildings*, *19*, 349-361.

Verma, R., Bansal, N. K., & Garg, H. P. (1986). The comparative performance of different approaches to passive cooling. *Building and Environment, 21* (2), 65-69.

VITA

Resume of Afzal Hossain
Phone: (480) 466-0772
Email: Afzal.Hossain@asu.edu

| ACADEMIC INFORMATION |

Year	Degree	Institution
2014	Ph. D.	Arizona State University (currently pursuing)
2013	M. Arch	University of Nevada Las Vegas
2006	B. Arch	Bangladesh University of Engineering & Technology

| WORK EXPERIENCES |

→ Teaching Assistant at the Arizona State University, from August 2010 till date.
→ Research Assistant at the Decision Theater, Arizona State University, from January 2011 till May 2012.
→ Graduate Research Assistant at the Natural Energies Advanced Technologies Laboratory (NEAT Lab), UNLV from August 2008 till May 2010.
→ Lecturer at the department of at the Architecture, Ahsanullah University of Science and Technology, from November 2007 till July 2008.
→ Graduate Teaching Assistant at the Department of Architecture, North South University from May 2007 till July 2008.
→ Assistant Architect at Profile Ltd, one of the largest architectural firms in Bangladesh, from November 2006 to April 2007.
→ Intern Architect at Architects' Design Center, from October 2005 to December 2005

| SCHOLARLY PUBLICATIONS |

Hossain, A. (2013). Development and validation of heat transfer model to predict indoor air temperatures in roofpond buildings. *Unpublished Masters' Thesis*. Las Vegas, NV: University of Nevada, Las Vegas.

Hossain, A., & Fernandez-Gonzalez, A. (2012). *Development and validation of a thermal network model to predict indoor operative temperatures in dry roofpond buildings*. Paper presented at the World renewable energy forum 2012, Denver, CO.

Fernandez-Gonzalez, A., & Hossain, A. (2010). *Cooling performance and energy savings produced by a roofpond in the United States Southwest*. Proceedings of the ASES National Solar Conference Phoenix: American Solar Energy Society.

Enam, K., & Hossain, A. (2007). *Search for an affordable shelter for urban poor*. Proceedings of the Architecture for economically disadvantaged Dhaka: Department of Architecture, BUET.

| SCHOLARSHIP & AWARDS |

Recipient of 2012 Anthony Juratovac Memorial Scholarship, ASU.
Best Student Paper (Honorable mention), WREF 2012 conference.
Recipient of 2010 SBSE Student Scholarship.
UNLV Graduate College Research Scholarship, spring 2010.
UNLV School of Architecture 2010 Research Excellence Award.
BUET Merit Scholarship for academic excellence, 2001-2006.

| ASSOCIATIONAL AFFILIATION |

Member of Society of Building Science Educators (SBSE).
Member of Golden Key International Honour Society.
Candidate Member of Institute of Architects, Bangladesh (IAB).
Student Representative, PhD in Design, Environment and the Arts Program at ASU.
President, Bangladeshi Students' Association at ASU.

| COMPUTER PROFICIENCY |

→ CADD/simulation: AutoCAD, SketchUp, 3ds Max, eQuest, AGi32, Ecotect, ArcGIS
→ Computer Graphics: Adobe Illustrator, Adobe Photoshop, Adobe Indesign, Adobe Flash, Adobe Dreamweaver, CorelDraw, Gimp
→ Office packages: MS Word, MS Excel, MS Powerpoint, MS Frontpage, MS Outlook
→ Statistical packages: IBM SPSS, StatGraphics Centurion, Minitab 15
→ Programing languages: AutoLISP, VBA for Excel

| ACADEMIC REFERENCES |

Alfredo Fernandez-Gonzalez
Associate Professor, School of Architecture
University of Nevada Las Vegas
Office: (702) 895-1141
Email: Alfredo.Fernandez@unlv.edu

Michael Kroelinger, PhD
Professor, The Design School
Arizona State University
Office: (480) 965-5561
Email: Michael.Kroelinger@asu.edu

Firas Al-Douri, PhD
Assistant Professor, School of Architecture
University of Nevada Las Vegas
Office: (702) 895-4880
Email: Firas.Al-Douri@unlv.edu

Harvey Bryan, PhD
Professor, The Design School
Arizona State University
Office: (480) 965-6094
Email: Harvey.Bryan@asu.edu